Acta Oceanol. Sin., 2022, Vol. 41, No. 9, P. 19–37
https://doi.org/10.1007/s13131-022-1998-0
http://www.aosocean.com
E-mail: ocean2@hyxb.org.cn

Contributions of shortwave radiation to the formation of temperature inversions in the Bay of Bengal and eastern equatorial Indian Ocean: A modeling approach

K M Azam Chowdhury[1, 2, 6], Wensheng Jiang[3]*, Changwei Bian[4, 5], Guimei Liu[6], Md Kawser Ahmed[2], Shaila Akhter[1, 7]

[1] College of Oceanic and Atmospheric Sciences, Ocean University of China, Qingdao 266100, China

[2] Department of Oceanography & International Centre for Ocean Governance (ICOG), University of Dhaka, Dhaka 1000, Bangladesh

[3] Key Lab of Marine Environment and Ecology of Ministry of Education, Ocean University of China, Qingdao 266100, China

[4] Frontiers Science Center for Deep Ocean Multispheres and Earth System (FDOMES), Ocean University of China, Qingdao 266100, China

[5] Pilot National Laboratory for Marine Science and Technology (Qingdao), Qingdao 266237, China

[6] National Marine Environmental Forecasting Center, Beijing 100081, China

[7] Bangladesh Betar, Ministry of Information and Broadcasting, Government of the People's Republic of Bangladesh, Dhaka 1207, Bangladesh

Received 22 August 2021; accepted 27 December 2021

Abstract

Variations in incoming shortwave radiation influence the net surface heat flux, contributing to the formation of a temperature inversion. The effects of shortwave radiation on the temperature inversions in the Bay of Bengal and eastern equatorial Indian Ocean have never been investigated. Thus, a high-resolution (horizontal resolution of 0.07°×0.07° with 50 vertical layers) Regional Ocean Modeling System (ROMS) model is utilized to quantify the contributions of shortwave radiation to the temperature inversions in the study domain. Analyses of the mixed layer heat and salt budgets are performed, and different model simulations are compared. The model results suggest that a 30% change in shortwave radiation can change approximately 3% of the temperature inversion area in the Bay of Bengal. Low shortwave radiation reduces the net surface heat flux and cools the mixed layer substantially; it also reduces the evaporation rate, causing less evaporative water vapor losses from the ocean than the typical situation, and ultimately enhances haline stratification. Thus, the rudimentary outcome of this research is that a decrease in shortwave radiation produces more temperature inversion in the study region, which is primarily driven by the net surface cooling and supported by the intensive haline stratification. Moreover, low shortwave radiation eventually intensifies the temperature inversion layer by thickening the barrier layer. This study could be an important reference for predicting how the Indian Ocean climate will respond to future changes in shortwave radiation.

Key words: mixed layer cooling, haline stratification, temperature inversion, ROMS model, shortwave radiation, Bay of Bengal, eastern equatorial Indian Ocean

Citation: Chowdhury K M Azam, Jiang Wensheng, Bian Changwei, Liu Guimei, Md Kawser Ahmed, Shaila Akhter. 2022. Contributions of shortwave radiation to the formation of temperature inversions in the Bay of Bengal and eastern equatorial Indian Ocean: A modeling approach. Acta Oceanologica Sinica, 41(9): 1–19, doi: 10.1007/s13131-022-1998-0

1 Introduction

A temperature inversion is characterized as a warm subsurface layer with a positive vertical temperature gradient. A strong haline stratified surface layer in the ocean creates a thin mixed layer with uniform density, recognized as the precursor for a temperature inversion (Shetye et al., 1996; Thompson et al., 2006; Hao et al., 2010). These inversions persist in conjunction with the barrier layer with a sharp salinity gradient below the thin mixed layer (Rao and Sastry, 1981; Rao et al., 1983; Thadathil et al., 2002; Kurian and Vinayachandran, 2006) and act as a barrier to the exchange of nutrients (Lukas and Lindstrom, 1991; Vinayachandran et al., 2002; Thadathil et al., 2007; de Boyer Montégut et al., 2007; He et al., 2020). Consequently, temperature inversions play a substantial role in influencing the climate system by modifying the sea surface temperature (SST) and heat in the mixed layer (Durand et al., 2004; Masson et al., 2002; Thompson et al., 2006; Thadathil et al., 2016; Kashem et al., 2019).

The Bay of Bengal and the eastern equatorial Indian Ocean (EEIO) comprise the tropical northeastern Indian Ocean. Because of its geographical setting, this region exhibits high incoming shortwave radiation and strong seasonal variations (Shenoi et al., 2002; Thangaprakash et al., 2016). However, the atmospheric

Foundation item: The Marine Scholarship of China, China Scholarship Council for International Doctoral Students under contract No. 2017SOA016552; the National Natural Science Foundation of China under contract Nos U2106204 and 41676003.
*Corresponding author, E-mail: wsjang@ouc.edu.cn

aerosol concentration and cloud cover above the Indian Ocean have increased from 1960 to 1990 (Ramanathan and Ramana, 2005; Yu et al., 2006), and the increased absorption and scattering of shortwave radiation by these aerosols and/or clouds has extensively reduced the amount of radiation that reaches the sea surface (Kaufman et al., 2005; Liao and Seinfeld, 1998; Haywood and Ramaswamy, 1998; Myhre and Myhre, 2003; Kim and Ramanathan, 2008). Recently, the shortwave radiation over the northern Indian Ocean has decreased by more than 14 W/m^2 (approximately 7% of the surface downwelling solar radiation over this region) (Ramanathan et al., 2001a, b; Kim et al., 2005; Ramanathan and Ramana, 2005; Yu et al., 2006). Such changes in shortwave radiation can affect the net surface heat flux through the air-sea interaction (Agarwal et al., 2007; Weller et al., 2016). Consequently, incoming shortwave radiation is the dominant influence on the seasonal SST pattern (Köberle and Philander, 1994; Thandlam and Rahaman , 2019) and the upper ocean thermal structure in this region. Hence, incoming shortwave radiation may contribute significantly to the formation of temperature inversions in the Bay of Bengal and EEIO. However, the relationship between the shortwave radiation and temperature inversions in this region has not yet been investigated.

In the Bay of Bengal, most previous observational (Rao et al., 1983, 1987; Suryanarayana et al., 1993; Thadathil et al., 2002, 2016; Vinayachandran et al., 2002; Li et al., 2012; Girishkumar et al., 2013; Chowdhury et al., 2019; Shee et al., 2019; He et al., 2020) and modeling studies (Babu and Rao, 2011; Nagura et al., 2015) on temperature inversions were performed either with limited stations or on small portions of the Bay of Bengal during a specific season. However, these studies did not explore the contributions of external forcings (e.g., river discharge, precipitation, and shortwave radiation) to the temperature inversion. Only Behara and Vinayachandran (2016) applied the Geophysical Fluid Dynamics Laboratory Modular Ocean Model (MOM4p1) to the entire Bay of Bengal with a horizontal resolution of 0.25°×0.25° and 40 vertical layers to study the contributions of river water and rainfall to the temperature inversion therein. Furthermore, the temperature inversion in the EEIO has scarcely been explored from both observational (Thompson et al., 2006; de Boyer Montégut et al., 2007) and modeling studies. Thus, the current study adopts a high-resolution (horizontal resolution of 0.07°×0.07° with 50 vertical layers) regional ocean model to quantify the role of shortwave radiation in the basin-wide distributions of the temperature inversion and its driving mechanisms in the Bay of Bengal and EEIO.

The remainder of this paper is arranged as follows: Section 2 describes the model setup and the forcing data; the methods used to analyze the mixed layer heat and salt budgets are also described. Section 3 validates the ability of the model simulation to capture the general oceanographic features and temperature inversions. Section 4 enumerates the distributions of the temperature inversion due to changes in shortwave radiation, and Section 5 describes the contribution of incoming shortwave radiation to the temperature inversion process. Finally, Section 6 concludes this study.

2 Model setup, datasets, and methods

The numerical model, its setup, the datasets utilized in the model, the model validation, and the methods used to analyze the results are described in this section. In this study, four seasons are considered following Thadathil et al. (2007) and Shee et al. (2019): winter (December–February), spring (March–May), summer (June–September), and autumn (October–November).

2.1 *Model description*

The ocean general circulation model used in this study is the Regional Ocean Modelling System (ROMS), a three-dimensional free-surface nonlinear model that solves the Reynolds-averaged Navier-Stokes equations using the hydrostatic and Boussinesq assumptions developed by Rutgers University, USA. (Danabasoglu et al., 1994; Haidvogel et al., 2000; Shchepetkin and McWilliams, 2003).

In this study, the model is configured for the Bay of Bengal and EEIO (5°S–23°N, 76°–98°E) (Fig. 1) with a high horizontal resolution of 7.8 km×7.8 km and 50 vertical layers. Parts of the eastern and western boundaries are open to the sea and thus kept open in the model. The southern boundary, which faces the open ocean, is also considered open. The radiation nudging condition is applied to transfer momentum in three dimensions. The vertical resolution is enhanced toward the surface by defining the s-coordinate stretching parameter as θ_S=7.0 at the surface and θ_B=0.1 at the bottom (Song and Haidvogel, 1994). In this configuration, a high vertical resolution within the upper 10 m (6 layers) and 100 m (18 layers) is used, which helps to analyze the near-surface processes with more confidence. The Mellor-Yamada Level 2.5 turbulence closure model represents vertical mixing (Mellor and Yamada, 1982). Jerlov water type IA (Jerlov, 1968), which corresponds to penetrative solar radiation is used. Although relaxation of the sea surface salinity (SSS) and SST allows the surface values to remain more realistic (Diansky et al., 2002; Sharma et al., 2010; Nyadjro et al., 2011), such relaxation artificially adds errors to the forcing or the model physics. Thus, it may be hazardous to conclude robust oceanic mechanisms in some locations of the Bay of Bengal (de Boyer Montégut, 2005). Therefore, no relaxation is applied to SST or SSS inside the domain.

In Fig. 1, the major rivers utilized in the model inputs are marked in dark blue. The black dashed line is the boundary between the Bay of Bengal and EEIO. SSS contours of 32.5 and 34 represent the southward extent of freshwater and the northward extent of saltier Arabian Sea water, respectively. The SSS contours are averaged for summer seasons (June to September) to show the dominant region of freshwater in the Bay of Bengal and

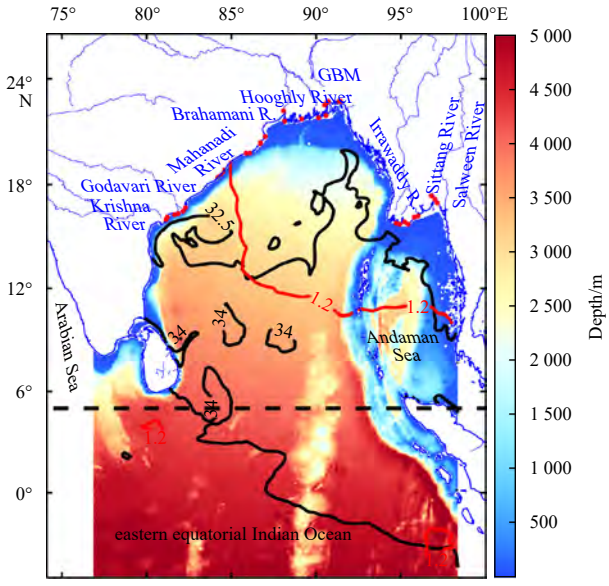

Fig. 1. Topography of the model domain in the Bay of Bengal and EEIO. GBM: Ganges-Brahmaputra-Meghna. The red points represent the 30 major river mouths along the coast. The red line means the contour line of the precipitation rate in kg/(m^2·s).

salty water in the EEIO. A precipitation contour of 1.2 kg/(m^2·s) represents the southward extent of the high rainfall zone during the summer monsoon.

2.2 *Forcing data*

The precise representation of rivers in a model remains a major challenge within the ocean modeling community, while it is relatively straightforward to address precipitation (Jensen et al., 2016; Jana et al., 2018). This study uses monthly discharge data from the Global River Discharge Database (Vorosmarty et al., 1998) and the Global Runoff Data Centre (Fekete et al., 2000). The total discharges of 11 rivers are divided and placed at 30 river points to establish a realistic geographical distribution of rivers flowing into this bay (Fig. 1). Notably, rivers are incorporated in the model through point sources across the coastal boundary, following Jana et al. (2015).

The tidal forcing is derived from the global TPXO8 tidal model and is prescribed along open boundaries using the amplitude and phase values of 8 tidal constituents (M_2, S_2, N_2, K_2, K_1, O_1, P_1, and Q_1) (Egbert and Erofeeva, 2002). The model is forced at the lateral open boundaries by the climatological potential temperature, salinity, horizontal velocity, and sea surface elevation obtained from the Simple Ocean Data Assimilation (SODA) dataset (Carton and Giese, 2008). The bottom topography is based on the ETOPO1 1-arcminute digital terrain model of the Earth's surface.

The model is initialized from rest on 1 January with the climatological temperature and salinity specified in the World Ocean Atlas 2009 (WOA09). We run the model for 15 years to ensure a stable spin-up with 3-hourly atmospheric fields obtained from the European Centre for Medium-Range Weather Forecasts (ECMWF) ERA-Interim dataset with a horizontal resolution of 0.125°×0.125° (Berrisford et al., 2009). The output on the last day is considered the initial condition for all subsequent simulations. The kinetic energy reaches dynamic equilibrium within 6 to 8 years, while both the temperature and the salinity take 10 to 12 years (figure not shown).

Notably, the ECMWF data used in the model include surface winds, radiation (shortwave and longwave), air temperature, air pressure, precipitation rate, and relative humidity. The latent and sensible heat fluxes, wind stresses, and evaporation are calculated inside the model using the standard bulk formulas of Fairall et al. (2003). After the 15-year spin-up run, the model is simulated for additional four years, from 2015 to 2018, using the previously obtained initial condition and all adopted forcing data, the results of which are taken as the good model climatology (hereafter, the Base simulation). Hence, the Base simulation is used for the model validation and further analysis in this study.

2.3 *Temperature and salinity gridded data*

This study uses a new version (EN.4.2.1) of the ocean objective analysis product (EN4) from the UK Met Office Hadley Centre, with temperature data from the Expendable Bathythermograph (XBT) corrected using the Gouretski and Reseghetti (2010) scheme. Here, the monthly gridded potential temperature and salinity fields are utilized, which have a horizontal resolution of 1° by 1° and a vertical resolution of 42 levels from the sea surface (~5 m) to 5 500 m. *In-situ* observations in the EN4 series came from the World Ocean Database (WOD13) (Boyer et al. 2013), the Global Temperature-Salinity Profile Program (GTSPP), the Array for Real-time Geostrophic Oceanography (Argo), and the Arctic Synoptic Basin-wide Observations (ASBO) (Levitus et al., 2009; Good et al., 2013). In this study, EN4 data from 2015 to 2018 is averaged and generated into a climatology to be compared with model climatology for the same years.

2.4 *Methods for analyzing the results*

2.4.1 *Temperature inversion-related parameters*

In recent studies, temperature thresholds of both 0.1°C (Girishkumar et al., 2013; Thadathil et al., 2016; Shee et al., 2019) and 0.2°C (Thompson et al., 2006; de Boyer Montégut et al., 2007; Li et al., 2016) were used to define the temperature inversions in the Bay of Bengal and the EEIO. This study chooses a minimum subsurface temperature increase of 0.2°C as the criterion for a temperature inversion. Otherwise, the profile is not considered to exhibit a temperature inversion. The topmost level in the model is 0 m. However, 5 m depth (as SST) was used to calculate the temperature inversion in both the model and observation (EN4 data), as the top level of EN4 data is about 5 m.

A decrease of 1°C in temperature from the surface (5 m) to the subsurface is set as the criterion to determine the isothermal layer depth (ILD, the layer with uniform temperature) for the case without a temperature inversion (Wyrtki et al., 1971; Masson et al., 2002; Monterey and Levitus, 1997; Thadathil et al., 2007, 2016; Shee et al., 2019). In the northern Bay of Bengal, temperature increases in the inversion profile of approximately 3°C to 4°C from the surface to the subsurface are common during winter (Thadathil et al., 2002). Thus, a drop of 1°C in the surface temperature overestimates the calculated ILD, as pointed out by Thadathil et al. (2007). Hence, Thadathil et al. (2007) regarded the surface as the upper limit of the ILD and the depth at which the temperature reaches the SST again as the lower limit of it. In this study, the definition of the ILD used by Thadathil et al. (2007) is adopted for the case with a temperature inversion.

The water density calculated from the model temperature and salinity data is used to calculate the mixed layer depth (MLD, the bottom depth of the mixed layer). To maintain consistency with the definition of the ILD (see Eq. (1)), the MLD is also calculated in terms of depth to a density equal to that at the surface plus a density increment equivalent to a 1°C decrease in temperature (Kara et al., 2000; Rao and Sivakumar, 2003; de Boyer Montégut et al., 2004; Thadathil et al., 2007; Kumari et al., 2018; He et al., 2020). Hence, the increment in the density is as follows:

$$\Delta\sigma = \sigma_t(\mathrm{SST} + \mathrm{d}T, \mathrm{SSS}, P_0) - \sigma_t(\mathrm{SST}, \mathrm{SSS}, P_0), \quad (1)$$

where $\Delta\sigma$ is the density difference between the surface and the MLD; σ_t is the potential density (kg/m^3) calculated from the temperature, salinity, and reference pressure (P_0); and dT is a 1°C increase in temperature. The barrier layer thickness (BLT) is the difference between the ILD and MLD.

The precise depth at which the subsurface temperature exceeds the SST by 0.02°C is defined as the initial inversion depth (i.e., the starting depth of the temperature inversion). The layer between the initial inversion depth and the bottom of the ILD is termed the temperature inversion layer. The temperature inversion intensity is determined by the thickness of the temperature inversion layer (hereafter, the thickness of the inversion layer), the depth of the peak temperature (i.e., the depth at which the subsurface temperature reaches the maximum), and the peak temperature. ΔT is the temperature difference between the peak temperature and SST, while ΔS is the salinity difference between the corresponding values at a depth of the peak temperature and the surface.

2.4.2 *Determining the water column stratification*

The Brunt-Väisälä frequency is the standard measure of the stratification tendency in a water column and can be calculated following the equation below (Roseli et al., 2015):

$$N^2 = -\frac{g}{\rho}\frac{\Delta\rho}{\Delta z}, \tag{2}$$

where N is the Brunt-Väisälä frequency, g is the gravitational constant of acceleration, ρ is the potential density, $\Delta\rho$ is the difference between the potential densities of two water parcels, and Δz is the vertical distance between the two water parcels. If N^2>0, the stratification is stable.

2.4.3 *Heat and salt budget calculations*

The heat and salt budget equations in the mixed layer at each grid point in the basin can be described by Eqs (3) and (4). Various terms contributing to the evolution of the temperature and salinity can be obtained by utilizing the "IAGNOSTICS_TS" option in the ROMS model (Vialard and Delecluse 1998; Vialard et al. 2008). These terms are averaged over the MLD and stored as monthly averages. Notably, the time resolution of the original model calculation is 4 min.

$$\underset{\text{(a)}}{\partial_t T_{\rm ml}} = \underset{\text{(b)}}{\frac{Q_{\rm net}-Q_{\rm pen}}{\rho C_{\rm p} h}} - \underset{\text{(c)}}{\frac{1}{h}\int_{-h}^{0} u\partial_x T\mathrm{d}z} - \underset{\text{(d)}}{\frac{1}{h}\int_{-h}^{0} v\partial_y T\mathrm{d}z} - \underset{\text{(e)}}{\frac{1}{h}\int_{-h}^{0} D_{\rm l}(T)\,\mathrm{d}z} + \underset{\text{(f)}}{H(W_{\rm d23}+\partial_t h)\frac{T_{h+5}-T_h}{h}} + \underset{\text{(g)}}{\frac{K_z}{h}\partial_z T} + \underset{\text{(h)}}{\text{remainder}}, \tag{3}$$

$$\underset{\text{(a)}}{\partial_t S_{\rm ml}} = \underset{\text{(b)}}{\frac{(E-P)S}{h}} - \underset{\text{(c)}}{\frac{1}{h}\int_{-h}^{0} u\partial_x S\mathrm{d}z} - \underset{\text{(d)}}{\frac{1}{h}\int_{-h}^{0} v\partial_y S\mathrm{d}z} - \underset{\text{(e)}}{\frac{1}{h}\int_{-h}^{0} D_{\rm l}(S)\,\mathrm{d}z} + \underset{\text{(f)}}{H(W_{\rm d23}+\partial_t h)\frac{S_{h+5}-S_h}{h}} + \underset{\text{(g)}}{\frac{K_z}{h}\partial_z S} + \underset{\text{(h)}}{\text{remainder}}. \tag{4}$$

Equations (3) and (4) represent the mixed layer heat and salt budgets, respectively. These equations include eight terms. Different terms in the mixed layer heat/salt budget analysis can contribute to the temperature/salinity changes in the mixed layer and hence help to explain the temperature inversion process (Thadathil et al., 2016; Li et al., 2016).

In Eq. (3) the term (a) represents the basin-averaged mixed layer temperature tendency, where $T_{\rm ml}$ is the mixed layer temperature at each grid point and $\partial_t T_{\rm ml}$ is the rate of change in the mixed layer temperature with respect to the month. T is the temperature at each grid point and varies with depth. Term (b) represents the mixed layer heat flux, where $Q_{\rm pen}$ is a model-derived penetrated component of solar radiation below the MLD, $Q_{\rm net}$ is the model net atmospheric heat flux, ρ is the seawater density (as a function of depth) calculated from the model temperature and salinity, $C_{\rm p}$ (3 989.2 J/(kg·°C)) is the specific heat capacity of seawater, and h is the model MLD (m). $Q_{\rm pen}$ is estimated as follows:

$$Q_{\rm pen} = 0.47 \times Q_{\rm short}[\nu_1 \mathrm{e}^{-\frac{h}{\xi_1}} + \nu_2 \mathrm{e}^{-\frac{h}{\xi_2}}], \tag{5}$$

where the incoming shortwave radiation ($Q_{\rm short}$) is corrected for the albedo at the sea surface (downwelling shortwave radiation is multiplied by 0.945), ν_1 and ν_2 are the partitioning factors (with $\nu_1+\nu_2=1$), and ξ_1 and ξ_2 are the attenuation depths of light at long visible, short visible and ultraviolet wavelengths (Morel and Antoine, 1994; Sweeney et al., 2005). The approximate values of ν_1, ν_2, ξ_1 and ξ_2 are 0.39, 0.69, 1.52, and 18.9, respectively (Morel and Antoine, 1994; Girishkumar et al., 2013).

Terms (c) and (d) are collectively called the horizontal advection term (temperature) along the zonal and meridional directions, and u and v are the zonal and meridional components, respectively, of the surface current. x and y indicate the longitudinal direction and latitudinal direction, respectively. Thus, the horizontal advection term is the combination of the longitudinal and latitudinal components (i.e., the sum of the terms (c) and (d)) of the surface current and its transport.

Here, the term (e) represents the lateral processes where $D_{\rm l}(\cdot)$ is the model lateral mixing operator (a parameterization of lateral mixing). Term (f) means vertical advection and vertical entrainment, where $W_{\rm d23}$ is the vertical velocity (m/month), which is the time rate of change in the 23°C isotherm depth (an indicator of the thermocline depth in the Bay of Bengal, Girishkumar et al., 2013) and is determined between the MLD and 5 m below the mixed layer (i.e., MLD+5), and $\partial_t h$ is the time rate of change in the MLD. The combination of $W_{\rm d23}$ and $\partial_t h$ is the resultant entrainment velocity (m/month) at the bottom of the mixed layer. H is the Heaviside step function (H=0 if $(W_{\rm d23}+\partial_t h)$<0 and H=1 if $(W_{\rm d23}+\partial_t h)$>0). Term (g) represents vertical diffusion, where $\partial_z T$ is the average vertical temperature gradient between the base of the mixed layer and 5 m below the MLD and the vertical diffusion coefficient K_z is considered to be 1 cm²/s. Hereafter, vertical advection, entrainment and diffusion (i.e., terms (f) and (g)) are collectively designated as vertical processes for convenience in this study.

Finally, the term (h) is called the remainder, which might contain measurement errors related to horizontal currents and surface heat fluxes, errors in parameterizing vertical processes, computational errors associated with finite differencing, and sampling errors (Foltz and McPhaden, 2009; Vialard et al., 2008; Halkides and Lee, 2011; Thadathil et al., 2016).

In Eq. (4), the term (a) represents the basin-averaged mixed layer salinity tendency, where $S_{\rm ml}$ is the mixed layer salinity, $\partial t S_{\rm ml}$ is the rate of change in the mixed layer salinity with respect to the month, and S is the salinity at each grid point and varies with depth. Term (b) represents the mixed layer freshwater flux term, where E, P, and S are the evaporation, precipitation, and salinity at each grid in this basin, respectively, and are derived from the model output. Terms (c) and (d) are collectively called the horizontal advection term (salinity). The other terms and parameters have meanings similar to those in Eq. (3).

3 Model validation

The northern Bay of Bengal (within 20°N to 22.5°N) and the adjacent Andaman Sea included in the study domain have insufficient *in situ* data (Akhil et al., 2014; Masud-Ul-Alam et al., 2020) because no Argo or mooring buoy data are presently available. Therefore, there are limited options to select an observational dataset to compare the model outputs in this region. In this study, the seasonal variations in the temperature (Figs 2 and 3), salinity (Figs 4 and 5), MLD (Fig. 6), and distribution of the temperature inversion (Fig. 7) from the model Base simulation are compared with the state-of-the-art EN4 climatology. The thermal and haline structures of the upper layer are vital for studying temperature inversions, and thus, validating the temperature, salinity, and MLD will yield confidence in this research.

3.1 *Temperature*

The spatial distribution of the seasonal SST and the vertical temperature profiles from the model Base simulation are compared with the EN4 data from the study area (Figs 2 and 3). The

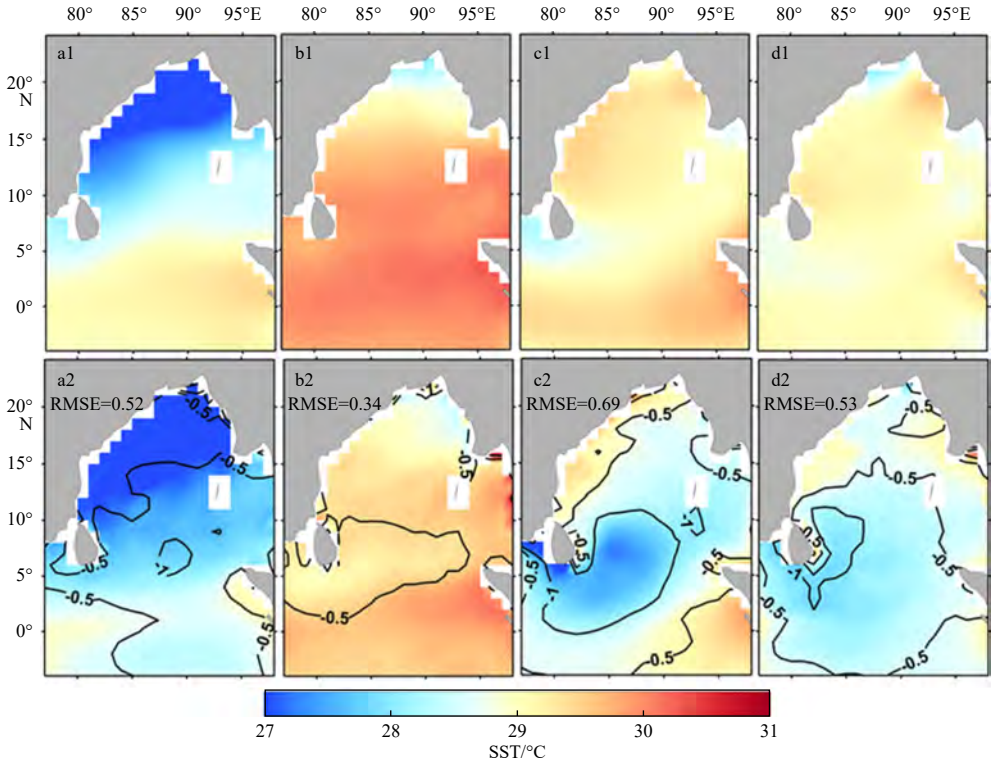

Fig. 2. Comparison of the sea surface temperature (SST) distributions in winter (a1, a2), spring (b1, b2), summer (c1, c2), and autumn (d1, d2) from the EN4 climatology (a1–d1) and model Base simulation (a2–d2). The contours in a2–d2 indicate the difference in the SST between the Base simulation and EN4 data.

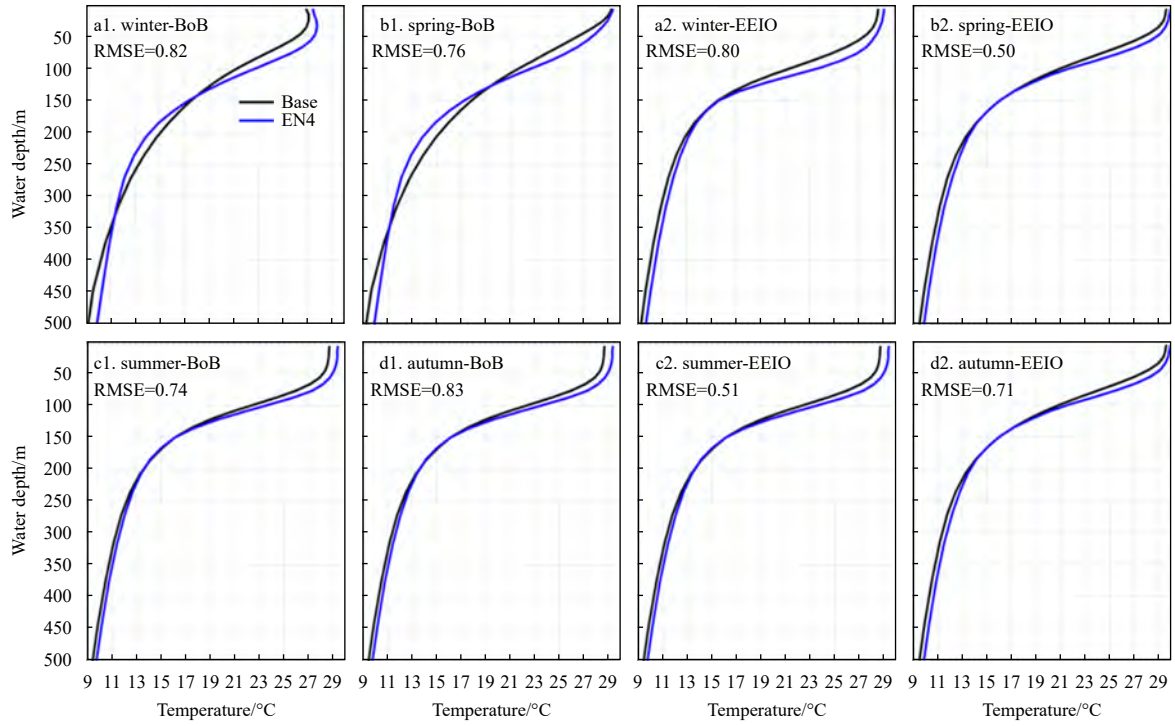

Fig. 3. Comparison of the area-averaged (separately for the Bay of Bengal (BoB) and eastern equatorial Indian Ocean (EEIO)) temperature profiles during winter (a1, a2), spring (b1, b2), summer (c1, c2), and autumn (d1, d2) from the EN4 data and the Base simulation.

model effectively reproduces the basin-wide seasonal SST distribution. Comparing the model-produced SST with the EN4 data yields basin averaged root-mean-square errors (RMSEs) ranging from 0.34°C to 0.69°C (Fig. 2). The highest SST bias (maximum

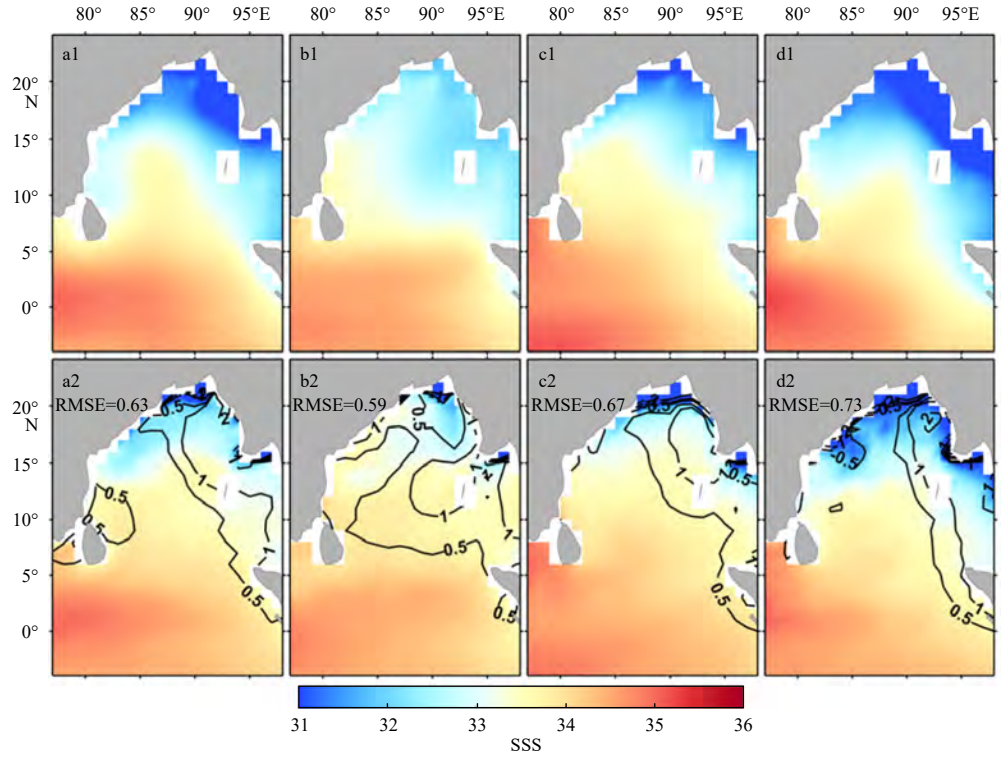

Fig. 4. Comparison of the sea surface salinity (SSS) distributions in winter (a1, a2), spring (b1, b2), summer (c1, c2) and autumn (d1, d2) from the EN4 climatology (a1–d1) and model Base simulation (a2–d2). The contours in a2–d2 indicate the difference in SSS between the Base simulation and EN4 data.

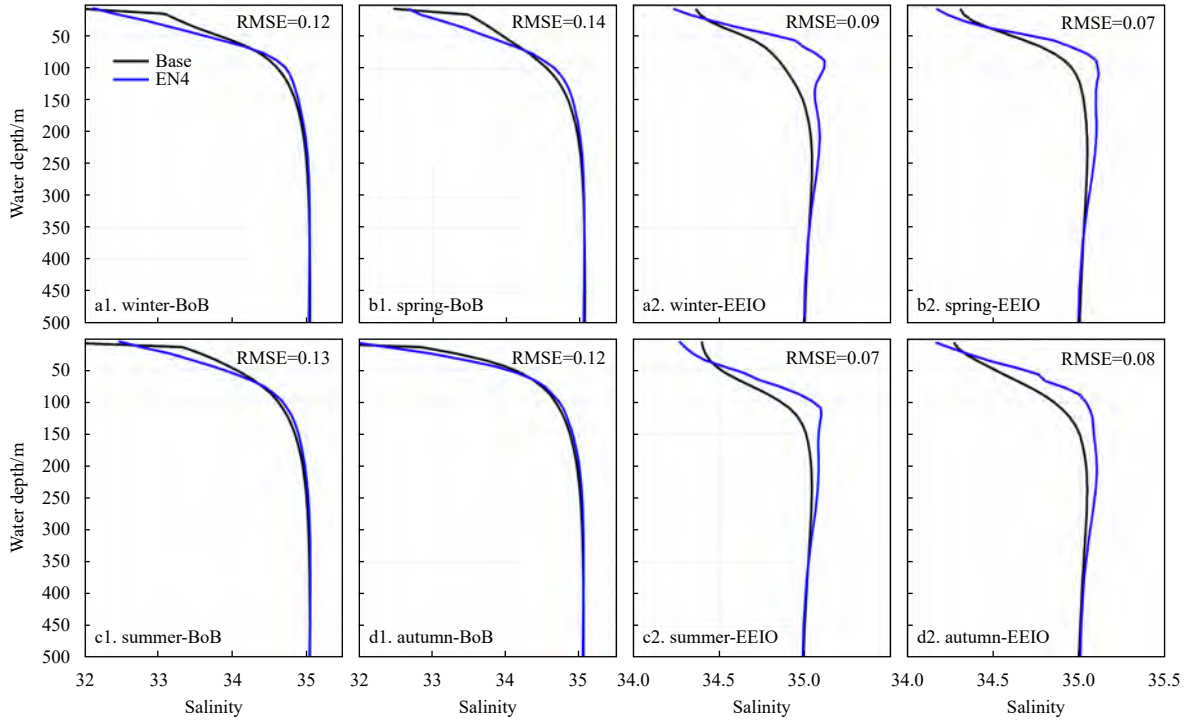

Fig. 5. Comparison of the area-averaged (separately for the Bay of Bengal (BoB) and eastern equatorial Indian Ocean (EEIO)) salinity profiles during winter (a1, a2), spring (b1, b2), summer (c1, c2), and autumn (d1, d2) from the EN4 data and the Base simulation.

1.5°C) occurs in the Sri Lanka dome (Fig. 2), known as a prominent upwelling region due to positive Ekman pumping (Vinayachandran and Yamagata, 1998; Vinayachandran, 2005). The EN4 data indicate that the SST in the EEIO is higher than that in the Bay of Bengal year-round, and the model Base simulation accurately captures this behavior. The model also reproduces the

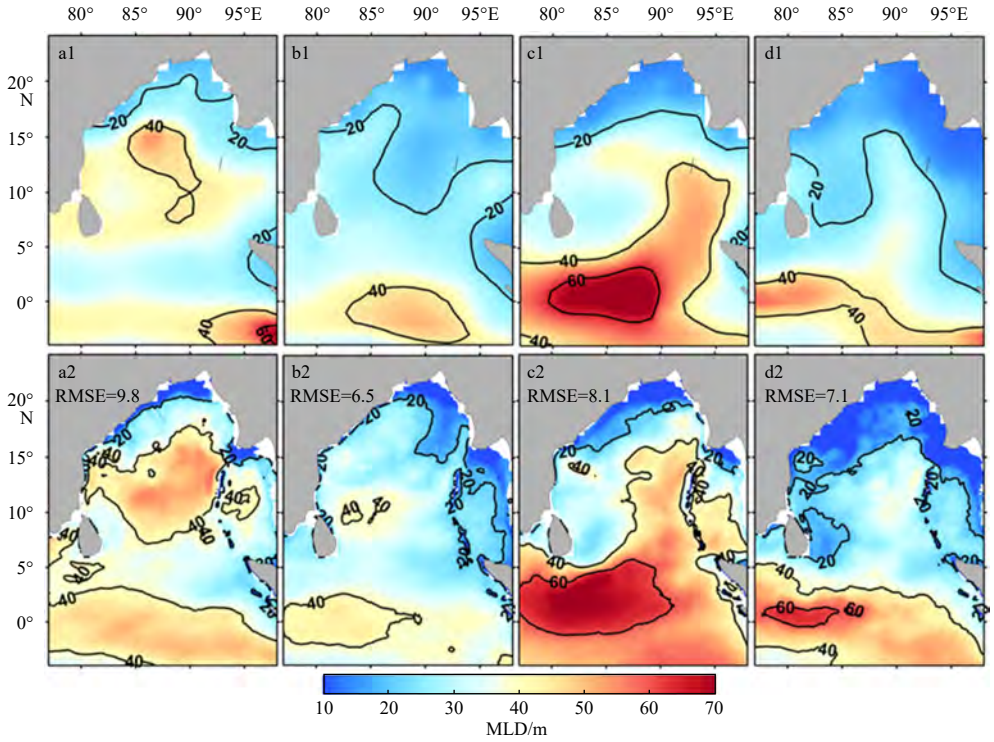

Fig. 6. Comparison of the mixed layer depth (MLD) (m) in winter (a1, a2), spring (b1, b2), summer (c1, c2), and autumn (d1, d2) from the EN4 data (a1–d1) and model Base simulation (a2–d2).

seasonal variation in the vertical temperature profiles; however, the subsurface temperature displays RMSEs of approximately 0.74°C to 0.83°C (Bay of Bengal) and 0.50°C to 0.80°C (EEIO) (Fig. 3). Remarkably, high RMSEs of 1.0°C to 2.3°C in the thermocline have also been reported using a high-resolution ROMS simulation in the Bay of Bengal (Chakraborty and Gangopadhyay, 2016). Furthermore, the model of Jana et al. (2015) overestimated the subsurface temperature (0.6°C), while our result shows a slight negative bias (~0.5°C). Hence, the error in the thermocline needs to be addressed in future studies, as precisely capturing the thermocline is still a significant challenge in the modeling community.

3.2 *Salinity*

The spatial distributions of SSS from both the model and the EN4 show lower salinity in the northern part of the bay than in the central and southern bay. The seasonal cycle is effectively reproduced by the model (Fig. 4). The extreme freshness (salinity less than 31) of the most significant freshwater contributor, the Ganges-Brahmaputra-Meghna (GBM) river system, is also accurately captured by the model Base simulation during summer and autumn, as are the freshwater inputs from the Irrawaddy, Sittang and Salween rivers into the northern Andaman Sea (Fig. 4). The intrusion of highly saline water from the Arabian Sea and its interaction with the fresher Bay of Bengal water during summer are prominent features in this domain (Vinayachandran et al., 2013; Jana et al., 2015). The intrusion of highly saline water from the Arabian Sea is also demonstrated by a strong surface salinity gradient between the eastern half of EEIO and other areas of the study domain, which can be seen in both the EN4 data and the model Base simulation (Fig. 4).

Moreover, the model reproduces the monthly variations in the basin-averaged salinity in both the surface (RMSE≈0.35) and the subsurface (RMSE≈0.04) layers (figure not shown). A similar bias was observed in Jana et al. (2018). During winter and spring, the model bias is relatively low (basin averaged RMSE ranges 0.59 to 0.63), but in summer and autumn, the salinity bias is slightly higher (RMSE≈0.75) (Fig. 4). The spatial SSS pattern depicts that this salinity bias exists throughout the year in the northeastern Bay of Bengal. These biases might be due to the underestimation of precipitation inputs forced in the model from the ECMWF data, as this area generally experiences high rainfall in the second half of the year (Sengupta et al., 2006; Akhil et al., 2014). The vertical profiles of the domain-averaged seasonal salinity are also in excellent agreement with the EN4 data, with a very small RMSE ranging from 0.07 to 0.09 (Bay of Bengal) and 0.12 to 0.14 (EEIO) (Fig. 5).

3.3 *MLD*

The mixed layer works as an interface between the ocean and the atmosphere. Therefore, the role of the mixed layer in the air-sea interaction is important, and the mixed layer regulates the thermohaline structure of the upper ocean (de Boyer Montégut et al., 2004; Mignot et al., 2007; Francis et al., 2013). Mixing in the upper thermohaline layer can disrupt the temperature inversion structure (He et al., 2020). In this section, the MLD calculated (see Eq. (1) in Section 2.4.1) from the model Base simulation is compared with the EN4 observational data (Fig. 6). In the study, the MLD is low during spring and autumn and comparatively high in winter, whereas it becomes the most elevated in summer; all of these behaviors are well captured by the model (Fig. 6).

The spatial distribution of the seasonal MLD is accurately captured year-round by the model Base simulation (the RMSE ranges from 6.5 m to 9.8 m) (Fig. 6). In the northern Bay of Bengal, a shallow MLD (depth less than 30 m) is observed throughout the year with slight seasonal variations, consistent with the findings of previous studies (Thadathil et al., 2007; Narvekar and Kumar, 2014). During autumn, the shallow MLD is

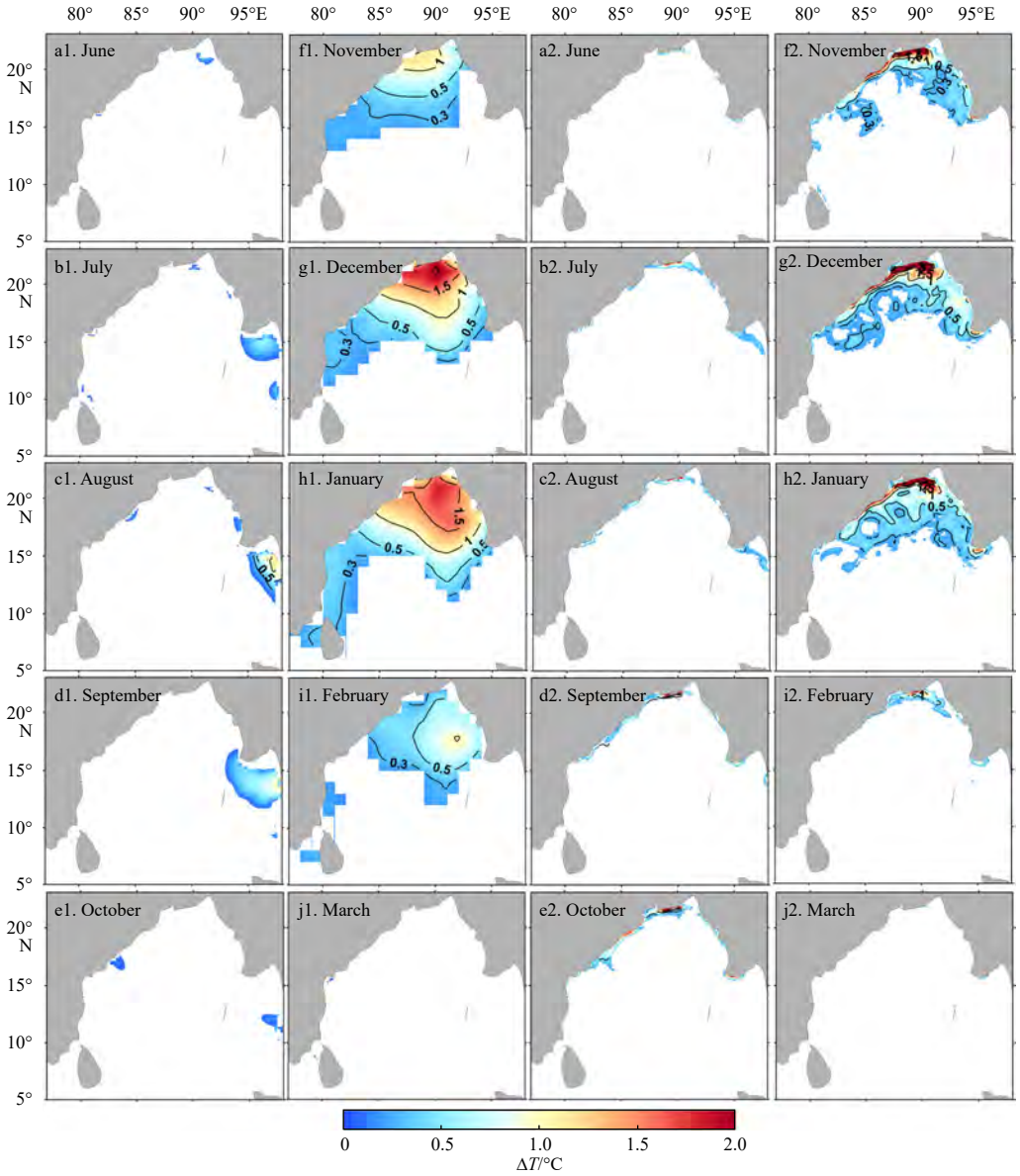

Fig. 7. Comparison of the spatial distributions of the temperature inversion (with contours of the monthly mean ΔT) for the EN4 (a1–j1) and model Base simulation (a2–j2).

due to freshwater-mediated haline stratification in the northern Bay of Bengal and precisely follows the advancement of the freshwater plume (Fig. 6d2), which has also been observed in previous studies (Rao and Sivakumar, 2003; Pant et al., 2015). During spring and autumn, weak transitional winds are observed (Shankar et al., 1996; Jana et al., 2018). However, in summer, highly saline water and strong wind-induced mixing continuously deepen the MLD, mainly in the EEIO and the southern Bay of Bengal in both the model Base simulation and the EN4 data (Figs 6c1, c2). Therefore, the model captures all of the seasonal features of the MLD in the Bay of Bengal and EEIO.

3.4 *Temperature inversion*

The monthly distributions of the temperature inversion in the Bay of Bengal derived from the model Base simulation are presented and compared with the monthly mean EN4 climatology (Fig. 7). The spatial and temporal distributions of the temperature inversion from the Base simulation indicate that the inversion starts to grow in June along the GBM river system and the Irrawaddy Estuary (Fig. 7a2). From July onward, the temperature inversion is additionally observed along the mouths of the Mahanadi and Krishna-Godavari rivers (Figs 7b2–d2). Subsequently, the temperature inversion spreads along the entire coastline north of 15°N until October, with ΔT varying from 0.2°C to 1.5°C (Fig. 7e2). From November to February of the following year, the inversion covers most of the northern Bay of Bengal with the highest ΔT of ~3.0°C (Figs 7f2–i2). The inversion almost disappears from March to May (Fig. 7j1). This spatial distribution produced by the Base simulation is nearly similar to the temperature inversion pattern derived from the EN4 climatological data (Fig. 7a1–j1). However, during summer, the model reproduces an inversion along the coastlines, but this distribution is not visible in the EN4 data because the temperature and salinity data of the EN4 do not cover the coastal region in the northern Bay of Bengal (Fig. 7). On the other hand, the model underestimates the surface area of the inversion by ~3% in winter compared with the EN4 data. Nevertheless, a winter temperature inversion was previously reported to be a permanent seasonal feature in the north-

ern Bay of Bengal (Li et al., 2016; Thadathil et al., 2016), and this feature is well captured in the model Base simulation. Hence, our model results strongly support the existence of a temperature inversion during summer at (17.5°N, 89°E), as was reported in an observational study (Vinayachandran et al., 2002).

Utilizing limited instantaneous Argo profile data, Thompson et al. (2006) and de Boyer Montégut et al. (2007) found some temperature inversions in the EEIO in different seasons. The daily averaged temperature inversion obtained by the model captures a similar feature (figure not shown), which is not visualized in the monthly averaged outputs. For instance, the daily distribution of the temperature inversion is discernible throughout the basin, even in spring. From April to July, the inversion extends into the eastern part of the EEIO. Therefore, the temperature inversion exists almost throughout the year in the Bay of Bengal and EEIO with substantial seasonal variation, which is more apparent in the daily distribution than in the monthly pattern. However, the features of the temperature inversions in the southern Bay of Bengal and EEIO occur at a smaller temporal scale (daily) than those in the northern part of the bay (both daily and monthly scale).

4 Role of shortwave radiation in temperature inversions

4.1 *Numerical experiments*

Two different model simulations are carried out to reveal the contribution of incoming shortwave radiation to the occurrence of the temperature inversion (Table 1). The same initial, open boundaries and atmospheric forcing conditions except for the shortwave radiation inputs are adopted in these simulations. Thereafter, simulations are performed by increasing and decreasing the incoming shortwave radiation by 30%. An increase in cloud cover and aerosol concentrations can scatter and reflect the incoming shortwave radiation (Ramanathan et al., 2001b; Yu et al., 2006). Thus, a 30% increase or decrease in shortwave radiation in the model simulation can be considered feasible because these amounts are not generally beyond the ranges of the maximum interannual/seasonal standard deviation in the Bay of Bengal.

4.2 *Distribution of the temperature inversion due to a change in shortwave radiation*

In the model domain, a decrease of 30% in shortwave radiation (SwrDec30) increases the surface area (~3%) of the temperature inversion in the northern Bay of Bengal. Nevertheless, the inversion layer follows a seasonal pattern similar to that in the

Table 1. List of model experiments

No.	Name of experiment	Meaning of the experiment
1	Base	no shortwave radiation
2	SwrInc30	30% increase of shortwave radiation
3	SwrDec30	30% decrease of shortwave radiation

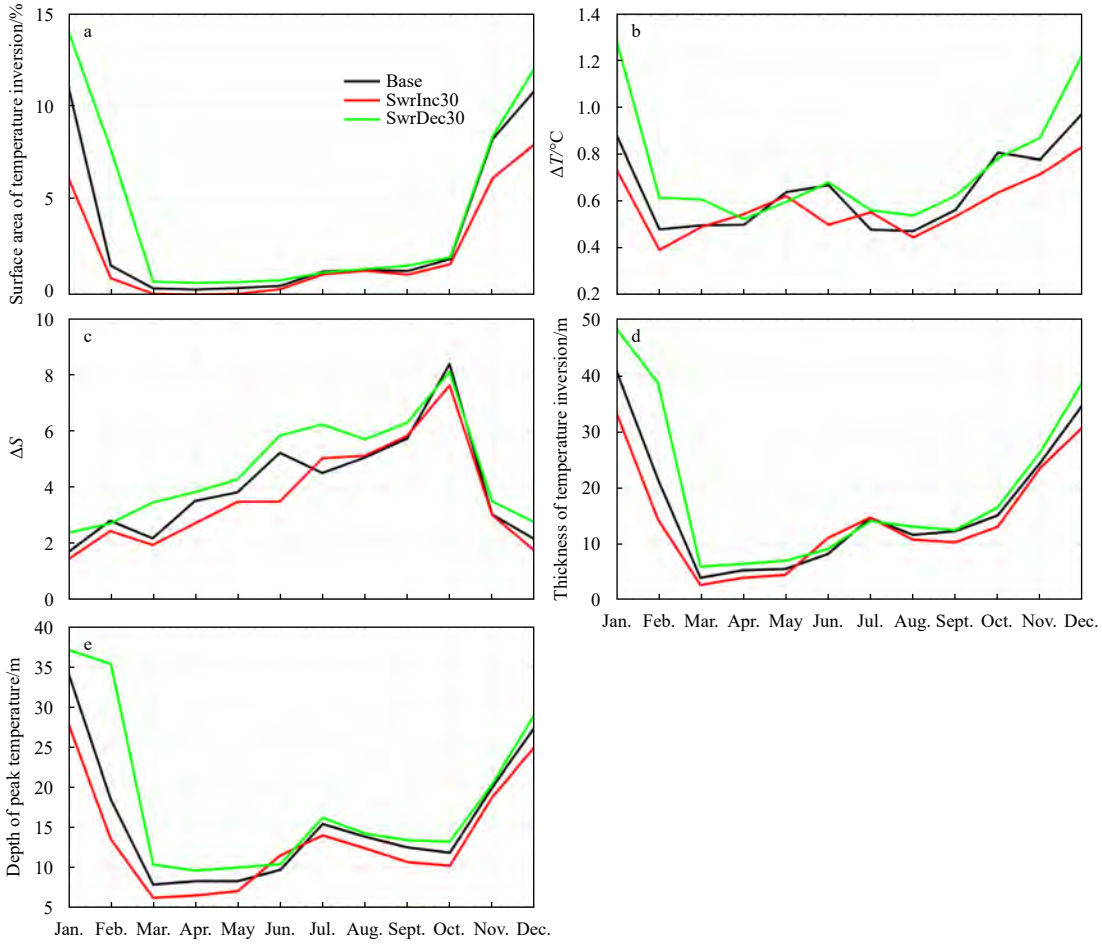

Fig. 8. Monthly variation in the surface area of the temperature inversion over study domain (a), regionally averaged (18°–22°N, 85°–95°E) monthly variations in ΔT (b) and in ΔS (c), thickness of the temperature inversion layer (d), and depth of the peak temperature (e) averaged over the study domain.

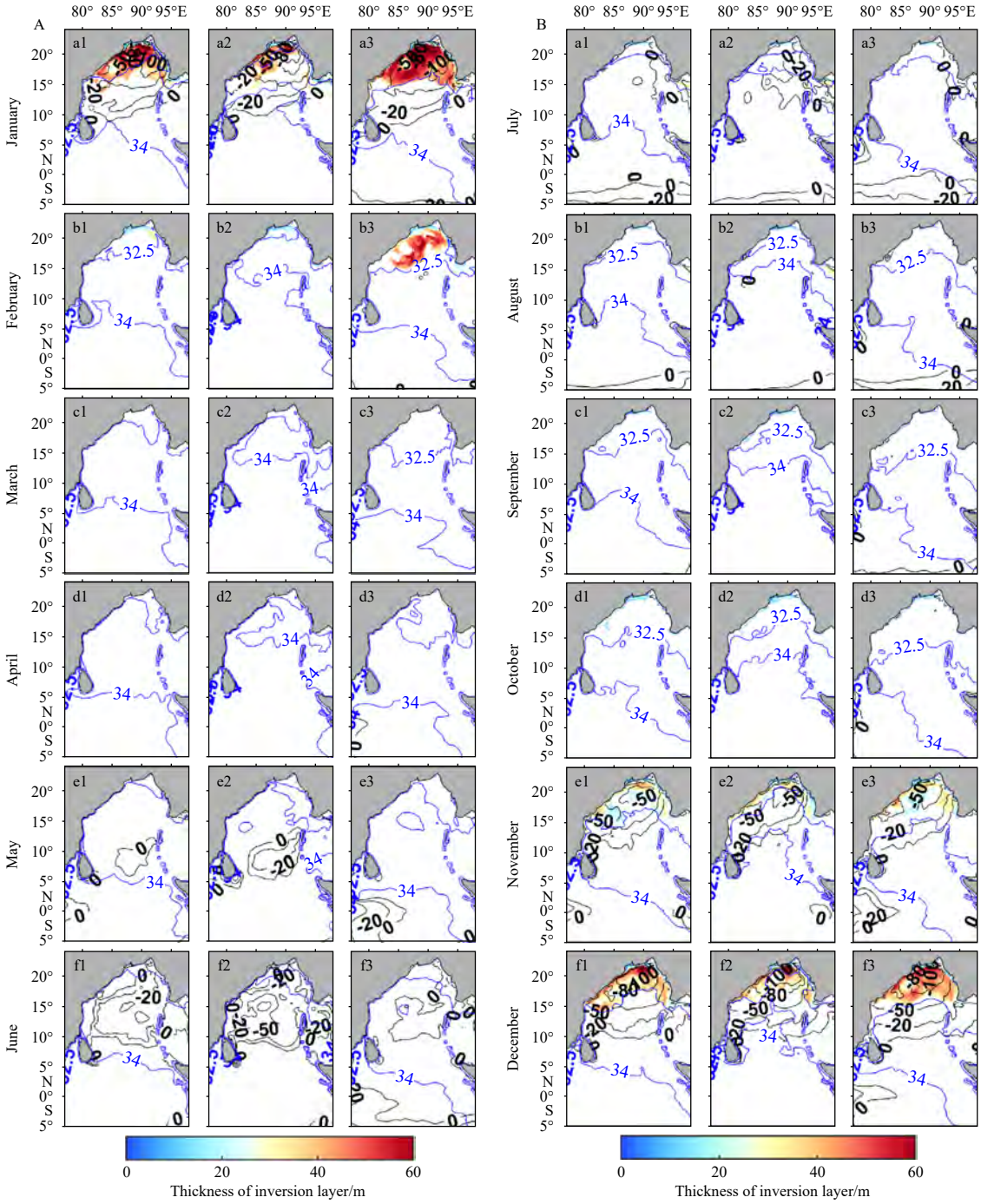

Fig. 9. Spatial distributions of the thickness of the temperature inversion from the Base simulation (a1–f1), SwrInc30 (a2–f2), and SwrDec30 (a3–f3) from January to December with contours of 32.5 and 34 for SSS (blue color) and for the net surface heat flux (0, –20, –50, –80, and –100, black color).

Base simulation, albeit with higher amplitude (Figs 8a and 9A, B column 3). In the SwrInc30 simulation, the temperature inversion also follows a similar seasonal pattern as the Base simulation, but the area of the temperature inversion is reduced in the northern Bay of Bengal. During winter, the surface area of the inversion decreases by ~2.5% compared with that in the Base simulation (Figs 8a and 9A, B column 2). Thus, a 30% change in shortwave radiation varies the temperature inversion by approximately 3% in the Bay of Bengal. Similar to the Base simulation, no inversions are observed in the EEIO in the SwrDec30 and SwrInc30 simulations on a monthly scale.

Regions of high ΔT and ΔS in the SwrDec30 and SwrInc30 simulations are observed along the northern coastal areas, similar to the Base simulation. However, an increase in shortwave radiation causes slight decreases in the amplitude of ΔT and ΔS (Figs 8b, c). Although the thickness of the inversion layer in the SwrInc30 simulation is slightly lower (~8 m) than that in the Base simulation, it is higher (~10 m) in the SwrDec30 simulation (Fig. 9). Furthermore, similar to the pattern of the inversion layer thickness, the distributions of the amplitude and seasonality of

the peak temperature depth are sensitive to changes in shortwave radiation (Figs 8d, e). Moreover, the surface area covered by the temperature inversion substantially increases with a decrease in shortwave radiation: its intensity is high during December and the subsequent January in the Base simulation (Figs 8 and 9). Therefore, changes in shortwave radiation significantly influence the temperature inversion characteristics both spatially and temporally in the Bay of Bengal. In particular, a decrease in shortwave radiation remarkably increases the surface area and intensity (i.e., the thickness of the inversion layer and the depth of the peak temperature) of the temperature inversion.

5 Major influencing mechanism of shortwave radiation on the temperature inversion

The four most probable driving processes governing the temperature inversion in the Bay of Bengal are net surface heat loss, haline stratification (Vinayachandran et al., 2002; Li et al., 2016; Thadathil et al., 2016; Shee et al., 2019), penetrative shortwave radiation below the mixed layer (Girishkumar et al., 2013), and thermocline deepening (He et al., 2020). The upper ocean thermohaline structure, MLD, and BLT can be affected by shortwave radiation, which changes these processes driving the formation and distribution of the temperature inversion. Analyses of the mixed layer heat and salt budgets from different simulations of the shortwave radiation for the Bay of Bengal (north of 5°N) and EEIO are conducted to improve our understanding of the mechanisms responsible for the temperature inversion (Figs 10–14). Moreover, the effect of shortwave radiation on the ILD, MLD, and BLT is explored at the end of this section (Fig. 15).

Precipitation and river discharge are the primary sources of freshwater in the Bay of Bengal (Murty et al., 1992; Shetye et al., 1996; Harenduprakash and Mitra, 1988; Sengupta et al., 2006; Chowdhury et al., 2021). This freshwater is responsible for the haline stratification and controls the salinity structure of this bay (Parampil et al., 2010; Chaitanya et al., 2014; Akhil et al., 2014; Akhter et al., 2021; Chowdhury et al., 2022). However, incoming shortwave radiation increases the surface temperature of the ocean, resulting in the occurrence of deep convection in the overlying atmosphere; this convective circulation accelerates evaporation (Rao and Sivakumar, 2000; Sengupta and Ravichandran, 2001; Shenoi et al., 2002), which converts seawater into water vapor and makes the ocean saltier (Thangaprakash et al., 2016). Therefore, shortwave radiation might significantly influence the salinity structure of the ocean through the air-sea interaction.

5.1 *Influence of the freshwater flux*

Although the input of freshwater (river discharge and precipitation) in the SwrDec30 simulation is similar to that in the Base simulation, a substantial reduction in surface salinity is observed (Fig. 10a). The mixed layer salt budget in the study region also shows that almost throughout the year, the mixed layer salinity variation and freshwater flux are remarkably lower (freshening)

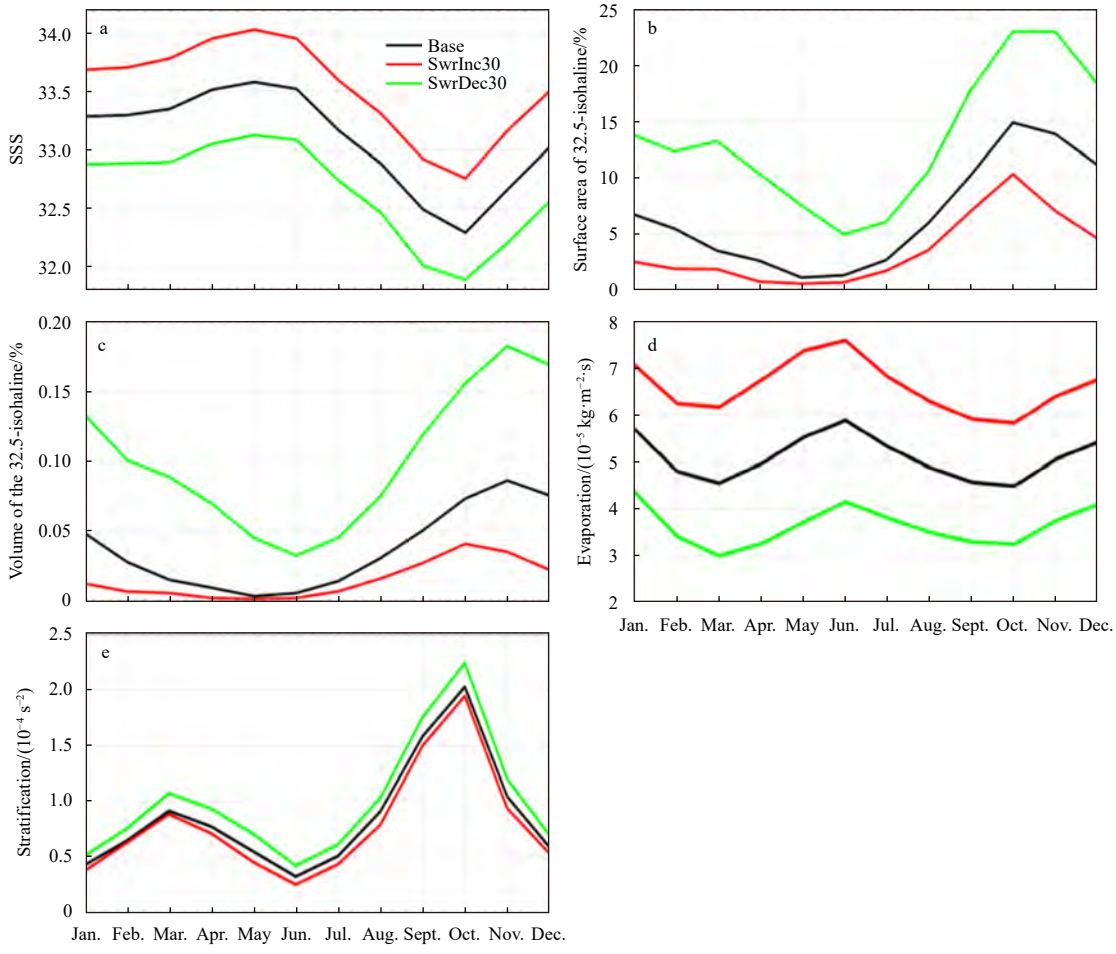

Fig. 10. Monthly variations in the area-averaged sea surface salinity (SSS) (a), surface area (b), volume of the freshwater plume region (c), evaporation (d), and stratification in the upper 10 m (e) averaged over the study domain.

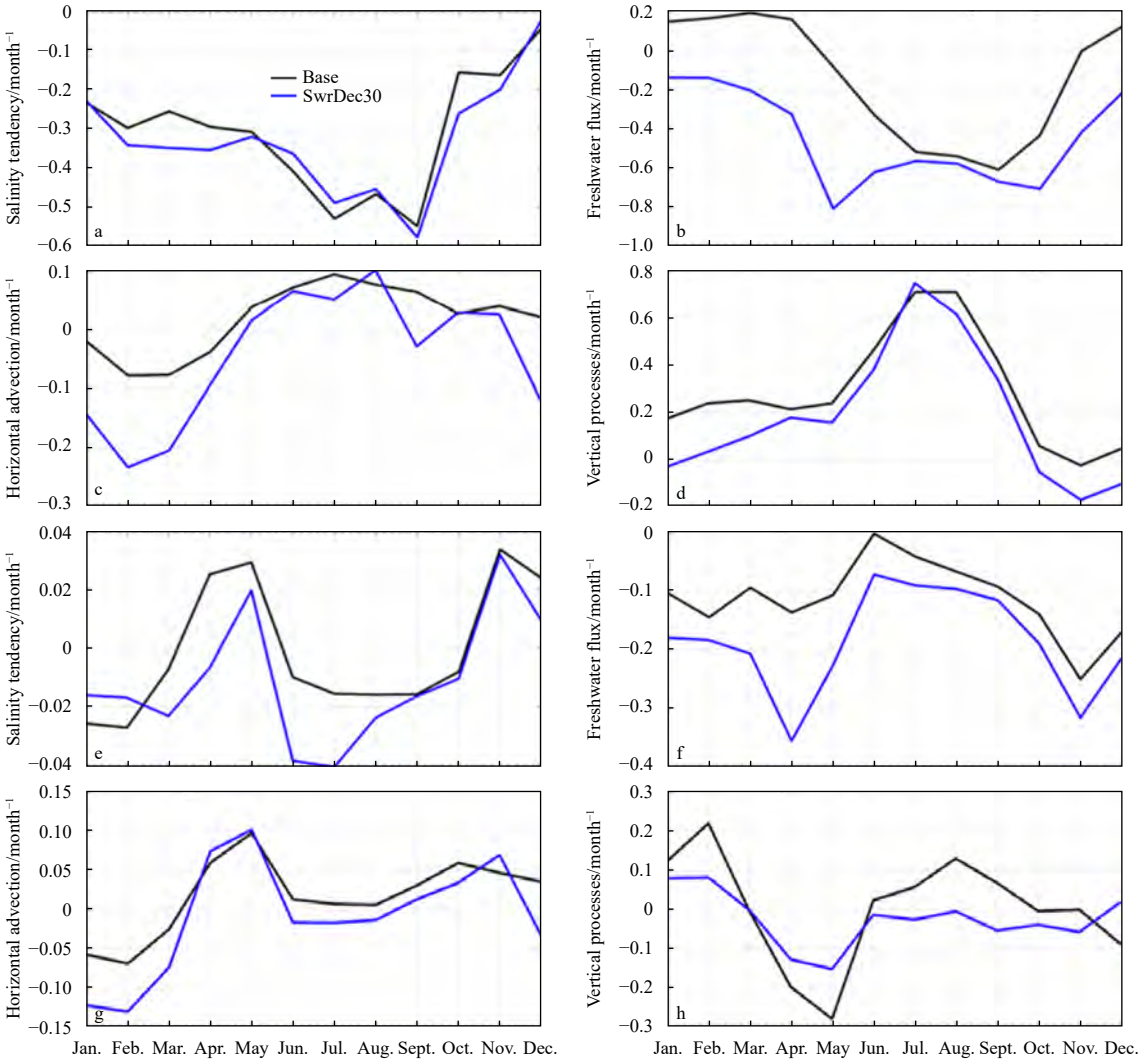

Fig. 11. Mixed layer salinity tendency (a, e), mixed layer freshwater flux (b, f), horizontal advection (c, g), and vertical processes (d, h) in the Bay of Bengal (a–d) and EEIO (e–h), respectively.

in the SwrDec30 simulation than in the Base simulation (Fig. 11), which is favorable for a temperature inversion. This low mixed layer freshwater flux is attributable to the reduced evaporation due to a decrease in shortwave radiation (Fig. 10d). Retardation of evaporation means a decrease of water vapor transfer from the ocean compared with the normal situation (Base simulation), and thus, the ocean contains more fresher water in the SwrDec30 simulation than that of Base simulation. In the SwrDec30 simulation, evaporation is reduced by approximately 30%, and the area of the freshwater plume increases proportionally, covering 7% more surface area than that in the Base simulation (Figs 10a, d). This freshwater plume is retained in the northern part of the bay, and the freshwater plume spreads more in autumn than in the other seasons following the seasonal cycle of the Base simulation (Figs 12a3–d3). In the SwrDec30 simulation, the freshwater plume is highly correlated with the spatial distributions of the temperature inversion and thickness of the inversion layer, which are higher in amplitude in this simulation than in the Base simulation (Fig. 8, columns 1 and 3 in Figs 9 and 12). In the northern Bay of Bengal, freshwater penetrates to deeper depths in the SwrDec30 and acquires more ocean volume than in the Base simulation (Figs 10a–c). Moreover, both ΔT and the inversion layer thickness are higher in the SwrDec30 simulation than in the Base simulation (Fig. 8). The vertical salinity processes also show comparatively fresher values in the SwrDec30 simulation than that of the Base simulation (Figs 11d, h).

On the other hand, with a 30% increase in shortwave radiation, evaporation increases by 28% compared with the Base simulation. The shortwave radiation input and freshwater plume also show an inverse relationship in the SwrInc30 simulation (Figs 12a2–d2). The area covered by the freshwater plume in the SwrInc30 simulation is inversely proportional to that in the SwrDec30 simulation, as are the temperature inversion and thickness of the inversion layer (Figs 8a, d, and Figs 12a1–d3). Therefore, a decrease in shortwave radiation significantly reduces the evaporation rate and exhibits low surface salinity compared with the typical situation. Consequently, low-salinity water-mediated haline stratification is correlated with the occurrence and intensity of a temperature inversion in the northern Bay of Bengal. However, the surface area of the inversion and the freshwater plume are not always coordinated in the Bay of Bengal. For instance, the freshwater plume is widespread, but temperature inversion is not much observed in October (Figs 9B d1–d3 and 12 d1–d3).

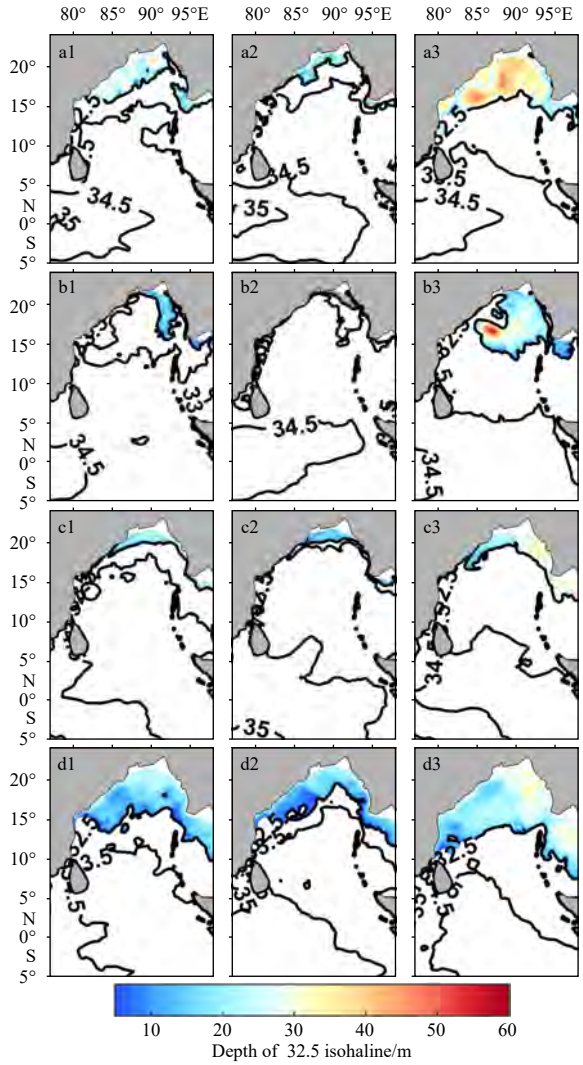

Fig. 12. Spatial distributions of the depth of the freshwater plume (i.e., depth of the 32.5-isohaline) in the Base (a1–d1), SwrInc30 (a2–d2), and SwrDec30 (a3–d3) simulations during January (a1–a3), April (b1–b3), July (c1–c3) and October (d1–d3).

5.2 *Net heat losses from ocean*

Due to a decrease in shortwave radiation (the SwrDec30 simulation), evaporation drops remarkably. Therefore, latent and sensible heat fluxes (Figs 13b, c) and net longwave radiation aid in transferring heat into the ocean. However, these three components of the net surface heat flux cannot increase the net surface heat; instead, the net surface heat flux reduces drastically because of the reduction of the dominant component, namely, incoming shortwave radiation (Fig. 13a).

In the SwrDec30 simulation, the net surface heat flux exhibits a semiannual peak with the highest value in spring and another peak in autumn. This seasonal pattern of the net surface heat flux is similar to that in the Base simulation, in which the flux values are comparatively low. Therefore, the surface area of the temperature inversion increases by ~3% compared with that in the Base simulation in the northern bay. In SwrInc30, the net surface heat flux increases, and thus, the temperature inversion decreases by ~2.5% from the Base simulation with a similar amplitude to the SwrDec30 simulation in this region.

The spatial distribution of the net surface heat flux indicates that the temperature inversion occurs in the area of the northern Bay of Bengal with low net heat flux, where fresher water (SSS<32.5) remains year-round in almost all the simulation (Fig. 9). Although some areas in the EEIO exhibit negative net surface heat flux, no temperature inversion occurs there. Saltier water (SSS ranges from ~33 to 35) might inhibit the formation of temperature inversion in the EEIO. The thickness of the inversion layer is also well correlated with the low net surface heat flux in the study domain (Fig. 9).

Furthermore, the roles of the mixed layer temperature tendency and its associated terms in controlling the temperature inversion are examined in the Bay of Bengal and EEIO using the SwrDec30 and Base simulations (Fig. 14). The mixed layer temperature tendency decreases in the SwrDec30 simulation year-round compared with the Base simulation in the Bay of Bengal (Fig. 14a). The mixed layer heat flux can clearly explain the low mixed layer temperature tendency, as they follow each other throughout the year in this bay (Figs 14a, b). The horizontal advection in the Bay of Bengal also exhibits a slightly cooling tendency in the SwrDec30 simulation than in the Base simulation. However, vertical processes show a slight warming tendency in the mixed layer compared to the Base simulation. This finding indicates the occurrence of subsurface warming and thus temperature inversion, which happens due to reduction in shortwave radiation (Figs 14c, d). Remarkably, the temporal pattern of the temperature inversion can be explained by the mixed layer temperature tendency in the Bay of Bengal. For instance, the occurrence and intensity of the temperature inversion are extremely high from November to next February, when the mixed layer temperature tendency also becomes considerably negative due to a decrease in shortwave radiation. The temperature inversion is significantly weaker in the remaining months when the mixed layer temperature tendency is high (warming). In the EEIO, the mixed layer heat flux is positive throughout the year, and thus, the mixed layer exhibits a warming tendency and no temperature inversion forms there (Figs 14e, f). The vertical processes in the EEIO also show a slight cooling tendency in the mixed layer in both the SwrDec30 and the Base simulation (Fig. 14h). Therefore, the net surface heat flux and thus low mixed layer heat flux-induced cooling exert the dominant controls on the temperature inversions in the Bay of Bengal, and incoming shortwave radiation plays an important role.

5.3 *Roles of the ILD and BLT in the thickness of the temperature inversion layer*

Deepening of the thermocline and the downwelling of Rossby and Kelvin waves can deepen the ILD (Wyrtki et al., 1971; Yu, 2003; Girishkumar et al., 2011; He et al., 2020). More incoming solar radiation thermally stratifies the upper layer, uplifts the thermocline, and shallows the ILD (Thadathil et al., 2007; Thangaprakash et al., 2016). As the BLT depends on the relative difference between the ILD and MLD, shallowing of the ILD makes the barrier layer thin. On the other hand, shallow MLD increases the BLT (Chowdhury et al., 2022). As the low shortwave radiation slows evaporation and enhances haline stratification, it results in shallower MLD in SwrDec30 simulation than Base (Fig. 15a).

In this study, all the simulations (Table 1), including the Base simulation, exhibit two peaks in the ILD: one in winter and another in summer (Fig. 15b). However, the BLT is the thickest only during winter (Fig. 15c). Interestingly, a deep ILD and a thick BLT during winter (Figs 15b, c) correlate well with an increased surface area and thickness (i.e., intensity) of the temperature inver-

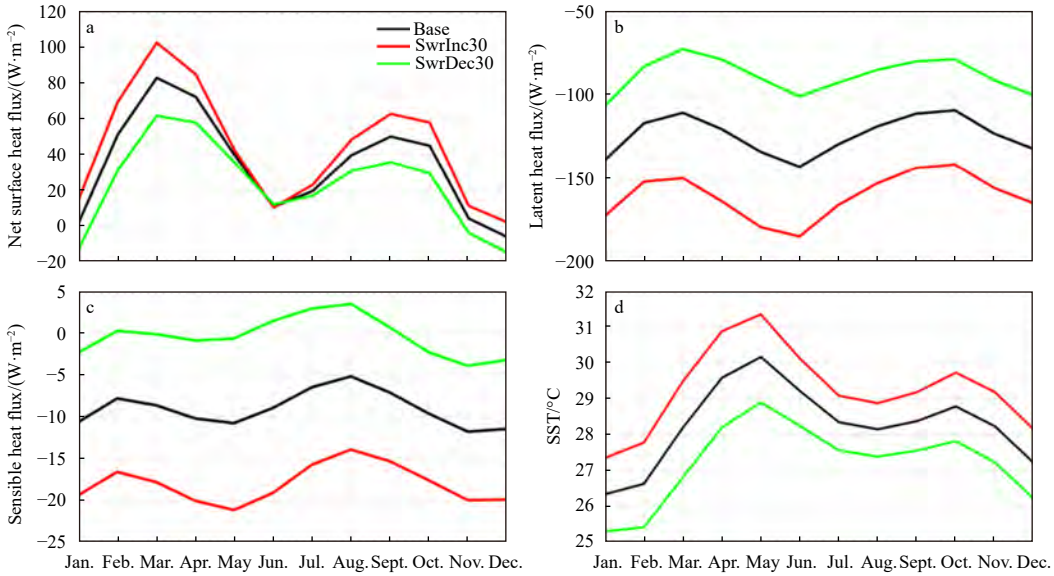

Fig. 13. Monthly variations in the area-averaged (study domain) net surface heat flux (a), latent heat flux (b), sensible heat flux (c), and sea surface temperature (SST) (d) in the different simulations.

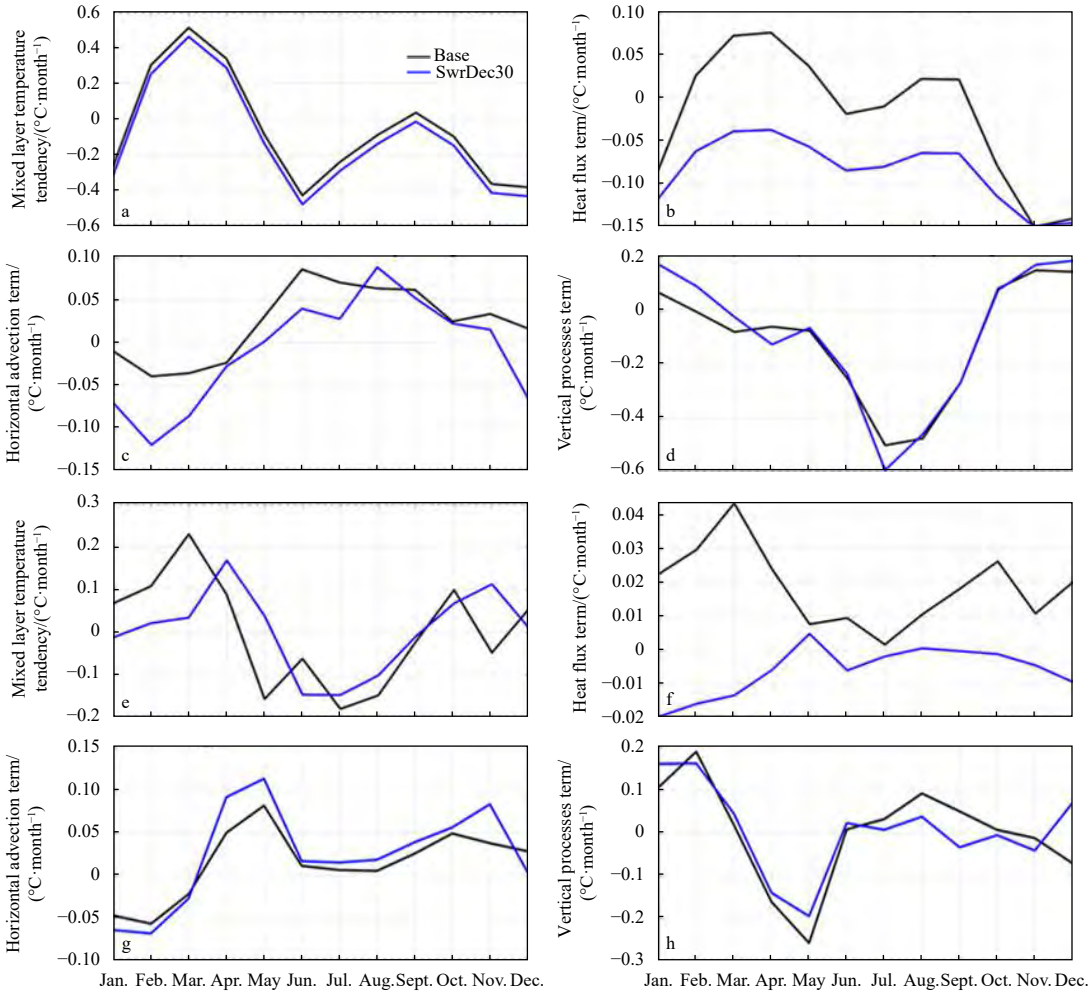

Fig. 14. Different terms in Eq. (3) in the Bay of Bengal (a–d) and EEIO (e–h). Mixed layer temperature tendency (a, e), heat flux term (b, f), horizontal advection term (c, g), and vertical processes term (d, h).

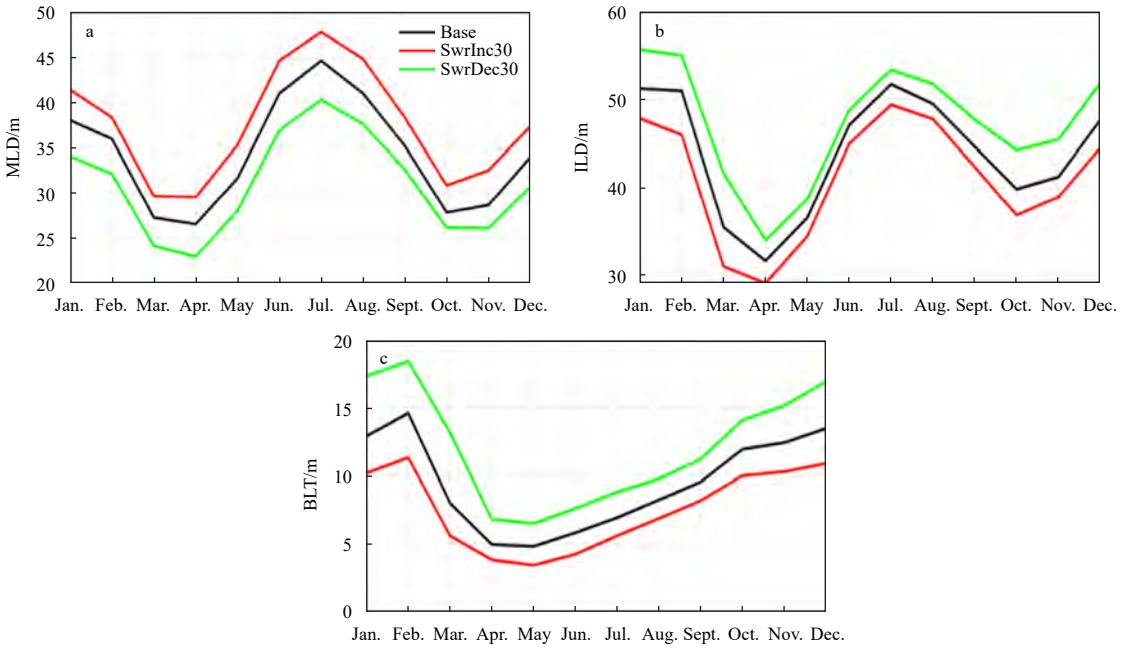

Fig. 15. Monthly variations in area-averaged (study domain) mixed layer depth (MLD) (a), isothermal layer depth (ILD) (b), and barrier layer thickness (BLT) (c).

sion layer in all these simulations (Figs 8 and 15). Especially in the northern Bay of Bengal, the intense temperature inversion during winter (Thadathil et al., 2007; Girishkumar et al., 2013) has similar relationships with the deep ILD and the thick BLT (Thadathil et al., 2007; Girishkumar et al., 2013). During summer, the basin-averaged ILD and MLD are both deep, and consequently, the BLT and inversion layer thickness is low (Figs 8a and 15).

In the SwrInc30 simulation (30% increase in shortwave radiation), the ILD is shallower, and thus, the BLT is thinner than that in the Base simulation (Figs 15b, c) due to the thermal stratification triggered by more incoming solar radiation. The thickness of the temperature inversion layer and the depth of the peak temperature are also lower than those in the Base simulation (Figs 8c, d). In contrast, a bit deeper ILD and a thicker BLT with a thicker temperature inversion layer are observed in the SwrDec30 simulation than in the Base simulation. The highest BLT occurs during winter and subsequent autumn when a thick temperature inversion layer prevails (Figs 8 and 15c). However, the formation of the temperature inversion depends on the haline stratification and cooling tendency in the mixed layer (see Sections 5.1 and 5.2). Moreover, a decrease in incoming shortwave radiation modestly deepens the ILD but significantly shoals the MLD, thickening the BLT and increasing the temperature inversion layer in the Bay of Bengal.

6 Conclusions

In addition to the effect of the air-sea interaction and other oceanic processes (e.g., horizontal advection and vertical processes), incoming shortwave radiation predominantly governs the seasonal extents and processes of the vertical temperature and salinity in the mixed layer (Shenoi et al., 2002; Thangaprakash et al., 2016). However, the roles of shortwave radiation in controlling the thermohaline structure and, consequently, the temperature inversion have not been explored previously. Thus, in this study, we quantify these roles for the Bay of Bengal and EEIO utilizing a high-resolution (horizontal resolution of 0.07°×0.07° with 50 vertical layers) ROMS model simulation. Accordingly, the seasonal patterns of the temperature, salinity, MLD, and temperature inversion are captured well by the model in the study region.

This study suggests that reducing the shortwave radiation reduces evaporation, which retards the hydrological cycle by reducing the transfer of water vapor from the ocean to the atmosphere. For instance, due to a 30% decrease in shortwave radiation, the area of a freshwater plume spreads ~10% more than in the typical situation. Consequently, fresher water reduces the salinity in the mixed layer and thus strengthens haline stratification, which is favorable for the formation of a temperature inversion. On the other hand, low evaporation and an increase in the sensible heat flux cannot fully compensate for the low incoming shortwave radiation-induced cooling in the ocean surface, which is also conducive to forming a temperature inversion (see the schematic in Fig. 16). Thus, a 30% change in shortwave radiation can vary the temperature inversion by approximately 3% in the study domain. Therefore, the key information is that due to reduction in shortwave radiation, net surface heat loss and consequent cooling in the mixed layer dominate the formation process of temperature inversions, and haline stratification supports this process. Changes in evaporation and subsequent modifications of the air-sea interaction exert the main controls on these mechanisms.

In addition, a decrease in shortwave radiation slightly deepens the ILD due to cooling in the upper layer of the ocean. At the same time, weaker evaporation strengthens the haline stratification due to fewer losses of water vapor compared to the typical situation, shallows the MLD and eventually enhances the BLT. Consequently, a 30% decrease in shortwave radiation increases the thickness of the temperature inversion layer by approximately 10 m. Thus, low shortwave radiation raises the thickness of the temperature inversion layer by increasing the BLT in the Bay of Bengal.

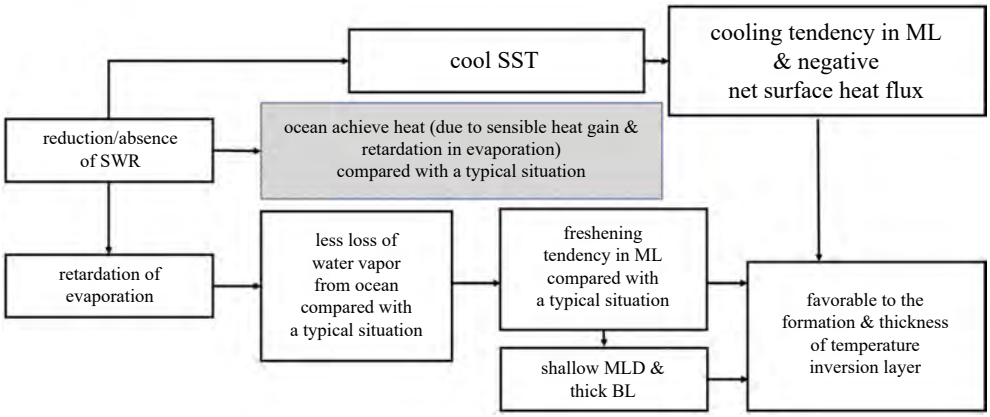

Fig. 16. A schematic describing the status of the thermohaline structure and temperature inversions in the Bay of Bengal due to variations in shortwave radiation. Here, SST stands for sea surface temperature; ML stands for the mixed layer; MLD stands for the mixed layer depth; BL stands for the barrier layer; SWR stands for shortwave radiation. The white and gray rectangles represent the favorable and unfavorable condition on the formation of the temperature inversion, respectively. The larger (smaller) effects were written in a larger (smaller) font.

References

Agarwal N, Sharma R, Basu S, et al. 2007. Bay of Bengal summer monsoon 10–20 day variability in sea surface temperature using model and observations. Geophysical Research Letters, 34(6): L06602, doi: 10.1029/2007GL029296

Akhil V P, Durand F, Lengaigne M, et al. 2014. A modeling study of the processes of surface salinity seasonal cycle in the Bay of Bengal. Journal of Geophysical Research: Oceans, 119(6): 3926–3947, doi: 10.1002/2013JC009632

Akhter S, Qiao Fangli, Wu Kejian, et al. 2021. Seasonal and long-term sea-level variations and their forcing factors in the northern Bay of Bengal: a statistical analysis of temperature, salinity, wind stress curl, and regional climate index data. Dynamics of Atmospheres and Oceans, 95: 101239, doi: 10.1016/j.dynatmoce.2021.101239

Babu S V, Rao A D. 2011. Mixing in the surface layers in association with internal waves during winter in the northwestern Bay of Bengal. Natural Hazards, 57(3): 551–562, doi: 10.1007/s11069-010-9607-5

Behara A, Vinayachandran P N. 2016. An OGCM study of the impact of rain and river water forcing on the Bay of Bengal. Journal of Geophysical Research: Oceans, 121(4): 2425–2446, doi: 10.1002/2015JC011325

Berrisford P, Dee D P, Fielding M, et al. 2009. The ERA-interim archive. Reading: European Centre for Medium-Range Weather Forecasts

Boyer T P, Antonov J I, Baranova O K, et al. 2013. World ocean database 2013. Silver Spring: NOAA

Carton J A, Giese B S. 2008. A reanalysis of ocean climate using simple ocean data assimilation (SODA). Monthly Weather Review, 136(8): 2999–3017, doi: 10.1175/2007MWR1978.1

Chaitanya A V S, Lengaigne M, Vialard J, et al. 2014. Salinity measurements collected by fishermen reveal a "river in the sea" flowing along the eastern coast of India. Bulletin of the American Meteorological Society, 95(12): 1897–1908, doi: 10.1175/BAMS-D-12-00243.1

Chakraborty A, Gangopadhyay A. 2016. Development of a high-resolution multiscale modeling and prediction system for Bay of Bengal, Part I: climatology-based simulations. Open Journal of Marine Science, 6(1): 145–176, doi: 10.4236/ojms.2016.61013

Chowdhury K M A, Jiang Wensheng, Liu Guimei, et al. 2019. Formation and types of thermal inversion in the Bay of Bengal. CLIVAR Exchanges, 76: 20–23

Chowdhury K M A, Jiang Wensheng, Liu Guimei, et al. 2021. Dominant physical-biogeochemical drivers for the seasonal variations in the surface chlorophyll-a and subsurface chlorophyll-a maximum in the Bay of Bengal. Regional Studies in Marine Science, 48: 102022, doi: 10.1016/j.rsma.2021.102022

Chowdhury K M A, Jiang Wensheng, Liu Guimei, et al. 2022. Spatiotemporal variation and mechanisms of temperature inversion in the Bay of Bengal and the eastern equatorial Indian Ocean. Acta Oceanologica Sinica, 41(4): 23–39, doi: 10.1007/s13131-021-1873-4

Danabasoglu G, McWilliams J C, Gent P R. 1994. The role of mesoscale tracer transports in the global ocean circulation. Science, 264(5162): 1123–1126, doi: 10.1126/science.264.5162.1123

de Boyer Montégut C. 2005. Couche mélangée océanique et bilan thermohalin de surface dans l'Océan Indien Nord (in French) [dissertation]. Paris: Universite Pierre et Marie Curie

de Boyer Montégut C, Madec G, Fischer A S, et al. 2004. Mixed layer depth over the global ocean: an examination of profile data and a profile-based climatology. Journal of Geophysical Research: Oceans, 109(C12): C12003, doi: 10.1029/2004jc002378

de Boyer Montégut C, Mignot J, Lazar A, et al. 2007. Control of salinity on the mixed layer depth in the world ocean: 1. General description. Journal of Geophysical Research: Oceans, 112(C6): C06011, doi: 10.1029/2006JC003953

Diansky N A, Bagno A V, Zalesny V B. 2002. Sigma model of global ocean circulation and its sensitivity to variations in wind stress. Izvestiya, Atmospheric and Oceanic Physics, 38(4): 477–494

Durand F, Shetye S R, Vialard J, et al. 2004. Impact of temperature inversions on SST evolution in the south-eastern Arabian Sea during the pre-summer monsoon season. Geophysical Research Letters, 31(1): L01305, doi: 10.1029/2003GL018906

Egbert G D, Erofeeva S Y. 2002. Efficient inverse modeling of barotropic ocean tides. Journal of Atmospheric and Oceanic Technology, 19(2): 183–204, doi: 10.1175/1520-0426(2002)019<0183:EIMOBO>2.0.CO;2

Fairall C W, Bradley E F, Hare J E, et al. 2003. Bulk parameterization of air-sea fluxes: updates and verification for the COARE algorithm. Journal of Climate, 16(4): 571–591, doi: 10.1175/1520-0442(2003)016<0571:BPOASF>2.0.CO;2

Fekete B M, Vörösmarty C J, Grabs W. 2000. Global composite runoff fields based on observed river discharge and simulated water balances. Koblenz, Germany: Global Runoff Data Centre

Foltz G R, McPhaden M J. 2009. Impact of barrier layer thickness on SST in the central tropical North Atlantic. Journal of Climate, 22(2): 285–299, doi: 10.1175/2008JCLI2308.1

Francis P A, Vinayachandran P N, Shenoi S S C. 2013. The Indian Ocean forecast system. Current Science, 104(10): 1354–1368

Girishkumar M S, Ravichandran M, McPhaden M J. 2013. Temperature inversions and their influence on the mixed layer heat budget during the winters of 2006–2007 and 2007–2008 in the Bay of Bengal. Journal of Geophysical Research: Oceans,

118(5): 2426–2437, doi: 10.1002/jgrc.20192
Girishkumar M S, Ravichandran M, McPhaden M J, et al. 2011. Intraseasonal variability in barrier layer thickness in the south central Bay of Bengal. Journal of Geophysical Research: Oceans, 116(C3): C03009, doi: 10.1029/2010JC006657
Good S A, Martin M J, Rayner N A. 2013. EN4: quality controlled ocean temperature and salinity profiles and monthly objective analyses with uncertainty estimates. Journal of Geophysical Research: Oceans, 118(12): 6704–6716, doi: 10.1002/2013JC009067
Gouretski V, Reseghetti F. 2010. On depth and temperature biases in bathythermograph data: development of a new correction scheme based on analysis of a global ocean database. Deep-Sea Research Part I: Oceanographic Research Papers, 57(6): 812–833, doi: 10.1016/j.dsr.2010.03.011
Haidvogel D B, Arango H G, Hedstrom K, et al. 2000. Model evaluation experiments in the North Atlantic Basin: simulations in nonlinear terrain-following coordinates. Dynamics of Atmospheres and Oceans, 32(3–4): 239–281, doi: 10.1016/s0377-0265(00)00049-x
Halkides D, Lee T. 2011. Mechanisms controlling seasonal mixed layer temperature and salinity in the southwestern tropical Indian Ocean. Dynamics of Atmospheres and Oceans, 51(3): 77–93, doi: 10.1016/j.dynatmoce.2011.03.002
Hao Jiajia, Chen Yongli, Wang Fan. 2010. Temperature inversion in China seas. Journal of Geophysical Research: Oceans, 115(C12): C12025, doi: 10.1029/2010JC006297
Harenduprakash L, Mitra A K. 1988. Vertical turbulent mass flux below the sea surface and air-sea interaction—monsoon region of the Indian Ocean. Deep-Sea Research Part A. Oceanographic Research Papers, 35(3): 333–346, doi: 10.1016/0198-0149(88)90014-3
Haywood J M, Ramaswamy V. 1998. Global sensitivity studies of the direct radiative forcing due to anthropogenic sulfate and black carbon aerosols. Journal of Geophysical Research: Atmospheres, 103(D6): 6043–6058, doi: 10.1029/97JD03426
He Qingyou, Zhan Haigang, Cai Shuqun. 2020. Anticyclonic eddies enhance the winter barrier layer and surface cooling in the Bay of Bengal. Journal of Geophysical Research: Oceans, 125(10): e16524, doi: 10.1029/2020JC016524
Jana S, Gangopadhyay A, Chakraborty A. 2015. Impact of seasonal river input on the Bay of Bengal simulation. Continental Shelf Research, 104: 45–62, doi: 10.1016/j.csr.2015.05.001
Jana S, Gangopadhyay A, Lermusiaux P F J, et al. 2018. Sensitivity of the Bay of Bengal upper ocean to different winds and river input conditions. Journal of Marine Systems, 187: 206–222, doi: 10.1016/j.jmarsys.2018.08.001
Jensen M P, Petersen W A, Bansemer A, et al. 2016. The midlatitude continental convective clouds experiment (MC3E). Bulletin of the American Meteorological Society, 97(9): 1667–1686, doi: 10.1175/BAMS-D-14-00228.1
Jerlov N G. 1968. Optical Oceanography. Amsterdam: Elsevier, 118–124
Kara A B, Rochford P A, Hurlburt H E. 2000. Mixed layer depth variability and barrier layer formation over the North Pacific Ocean. Journal of Geophysical Research: Oceans, 105(C7): 16783–16801, doi: 10.1029/2000JC900071
Kashem M, Ahmed M K, Qiao Fangli, et al. 2019. The response of the upper ocean to tropical cyclone Viyaru over the Bay of Bengal. Acta Oceanologica Sinica, 38(1): 61–70, doi: 10.1007/s13131-019-1370-1
Kaufman Y J, Koren I, Remer L A, et al. 2005. The effect of smoke, dust, and pollution aerosol on shallow cloud development over the Atlantic Ocean. Proceedings of the National Academy of Sciences of the United States of America, 102(32): 11207–11212, doi: 10.1073/pnas.0505191102
Kim D, Ramanathan V. 2008. Solar radiation budget and radiative forcing due to aerosols and clouds. Journal of Geophysical Research: Atmospheres, 113(D2): D02203, doi: 10.1029/2007JD008434
Kim D H, Sohn B J, Nakajima T, et al. 2005. Aerosol radiative forcing over East Asia determined from ground-based solar radiation measurements. Journal of Geophysical Research: Atmospheres, 110(D10): D10S22, doi: 10.1029/2004JD004678
Köberle C, Philander S G H. 1994. On the processes that control seasonal variations of sea surface temperatures in the tropical Pacific Ocean. Tellus A: Dynamic Meteorology and Oceanography, 46(4): 481–496, doi: 10.3402/tellusa.v46i4.15494
Kumari A, Kumar S P, Chakraborty A. 2018. Seasonal and interannual variability in the barrier layer of the Bay of Bengal. Journal of Geophysical Research: Oceans, 123(2): 1001–1015, doi: 10.1002/2017JC013213
Kurian J, Vinayachandran P N. 2006. Formation mechanisms of temperature inversions in the southeastern Arabian Sea. Geophysical Research Letters, 33(17): L17611, doi: 10.1029/2006GL027280
Levitus S, Antonov J I, Boyer T P, et al. 2009. Global ocean heat content 1955–2008 in light of recently revealed instrumentation problems. Geophysical Research Letters, 36(7): L07608, doi: 10.1029/2008GL037155
Li Kuiping, Wang Haiyuan, Yang Yang, et al. 2016. Observed characteristics and mechanisms of temperature inversion in the northern Bay of Bengal. Haiyang Xuebao (in chinese), 38(7): 22–31
Li Jian, Yang Lei, Shu Yeqiang, et al. 2012. Temperature inversion in the Bay of Bengal prior to the summer monsoon onsets in 2010 and 2011. Atmospheric and Oceanic Science Letters, 5(4): 290–294, doi: 10.1080/16742834.2012.11447004
Liao H, Seinfeld J H. 1998. Radiative forcing by mineral dust aerosols: sensitivity to key variables. Journal of Geophysical Research: Atmospheres, 103(D24): 31637–31645, doi: 10.1029/1998JD200036
Lukas R, Lindstrom E. 1991. The mixed layer of the western equatorial Pacific Ocean. Journal of Geophysical Research: Oceans, 96(S01): 3343–3357, doi: 10.1029/90JC01951
Masson S, Delecluse P, Boulanger J P, et al. 2002. A model study of the seasonal variability and formation mechanisms of the barrier layer in the eastern equatorial Indian Ocean. Journal of Geophysical Research: Oceans, 107(C12): 8017, doi: 10.1029/2001JC000832
Masud-Ul-Alam M, Khan M A I, Sunny S K, et al. 2020. An exclusive *in-situ* dataset on physicochemical parameters in the Gappy northern Bay of Bengal. Data in Brief, 31: 106024, doi: 10.1016/j.dib.2020.106024
Mellor G L, Yamada T. 1982. Development of a turbulence closure model for geophysical fluid problems. Reviews of Geophysics, 20(4): 851–875, doi: 10.1029/RG020i004p00851
Mignot J, de Boyer Montégut C, Lazar A, et al. 2007. Control of salinity on the mixed layer depth in the world ocean: 2. Tropical areas. Journal of Geophysical Research: Oceans, 112(C10): C10010, doi: 10.1029/2006JC003954
Monterey G I, Levitus S. 1997. Seasonal variability of mixed layer depth for the world ocean. Silver Spring: NOAA
Morel A, Antoine D. 1994. Heating rate within the upper ocean in relation to its bio-optical state. Journal of Physical Oceanography, 24(7): 1652–1665, doi: 10.1175/1520-0485(1994)024<1652:HRWTUO>2.0.CO;2
Murty V S N, Sarma Y V B, Babu M T, et al. 1992. Hydrography and circulation in the northwestern Bay of Bengal during the retreat of southwest monsoon. Proceedings of the Indian Academy of Sciences-Earth and Planetary Sciences, 101: 67–75, doi: 10.1007/BF02839173
Myhre G, Myhre A. 2003. Uncertainties in radiative forcing due to surface albedo changes caused by land-use changes. Journal of Climate, 16(10): 1511–1524, doi: 10.1175/1520-0442(2003)016<1511:UIRFDT>2.0.CO;2
Nagura M, Terao T, Hashizume M. 2015. The role of temperature inversions in the generation of seasonal and interannual SST variability in the far northern Bay of Bengal. Journal of Climate, 28(9): 3671–3693, doi: 10.1175/JCLI-D-14-00553.1
Narvekar J, Kumar S P. 2014. Mixed layer variability and chlorophyll *a* biomass in the Bay of Bengal. Biogeosciences, 11(14): 3819–3843, doi: 10.5194/bg-11-3819-2014

Nyadjro E S, Subrahmanyam B, Shriver J F. 2011. Seasonal variability of salt transport during the Indian Ocean monsoons. Journal of Geophysical Research: Oceans, 116(C8): C08036, doi: 10.1029/2011JC006993

Pant V, Girishkumar M S, Bhaskar T V S U, et al. 2015. Observed interannual variability of near-surface salinity in the Bay of Bengal. Journal of Geophysical Research: Oceans, 120(5): 3315–3329, doi: 10.1002/2014JC010340

Parampil S R, Gera A, Ravichandran M, et al. 2010. Intraseasonal response of mixed layer temperature and salinity in the Bay of Bengal to heat and freshwater flux. Journal of Geophysical Research: Oceans, 115(C5): C05002, doi: 10.1029/2009JC005790

Ramanathan V, Crutzen P J, Kiehl J T, et al. 2001a. Aerosols, climate, and the hydrological cycle. Science, 294(5549): 2119–2124, doi: 10.1126/science.1064034

Ramanathan V, Crutzen P J, Lelieveld J, et al. 2001b. Indian Ocean experiment: an integrated analysis of the climate forcing and effects of the great Indo-Asian haze. Journal of Geophysical Research: Atmospheres, 106(D22): 28371–28398, doi: 10.1029/2001JD900133

Ramanathan V, Ramana M V. 2005. Persistent, widespread, and strongly absorbing haze over the Himalayan foothills and the Indo-Gangetic plains. Pure and Applied Geophysics, 162(8): 1609–1626

Rao B P, Babu V R, Chandramohan P. 1987. Seasonal and diurnal variability of thermal structure in the coastal waters off Visakhapatnam. Proceedings of the Indian Academy of Sciences-Earth and Planetary Sciences, 96(1): 69–79, doi: 10.1007/BF02842639

Rao R R, Rao D S, Murthy P G K, et al. 1983. A preliminary investigation of the summer monsoonal forcing on the thermal structure of upper Bay of Bengal during Monex-79. Mausum, 32: 85–92

Rao D P, Sastry J S. 1981. Circulation and distribution of some hydrographical properties during the late winter in the Bay of Bengal. Mahasagar, 14(1): 1–15

Rao R R, Sivakumar R. 2000. Seasonal variability of near-surface thermal structure and heat budget of the mixed layer of the tropical Indian Ocean from a new global ocean temperature climatology. Journal of Geophysical Research: Oceans, 105(C1): 995–1015, doi: 10.1029/1999JC900220

Rao R R, Sivakumar R. 2003. Seasonal variability of sea surface salinity and salt budget of the mixed layer of the north Indian Ocean. Journal of Geophysical Research: Oceans, 108(C1): 3009, doi: 10.1029/2001JC000907

Roseli N H, Akhir M F, Husain M L, et al. 2015. Water mass characteristics and stratification at the shallow Sunda shelf of southern South China Sea. Open Journal of Marine Science, 5(4): 455–467, doi: 10.4236/ojms.2015.54036

Sengupta D, Raj G N B, Shenoi S S C. 2006. Surface freshwater from Bay of Bengal runoff and Indonesian throughflow in the tropical Indian Ocean. Geophysical Research Letters, 33(22): L22609, doi: 10.1029/2006GL027573

Sengupta D, Ravichandran M. 2001. Oscillations of Bay of Bengal sea surface temperature during the 1998 summer monsoon. Geophysical Research Letters, 28(10): 2033–2036, doi: 10.1029/2000GL012548

Shankar D, McCreary J P, Han W, et al. 1996. Dynamics of the East India coastal current: 1. Analytic solutions forced by interior Ekman pumping and local alongshore winds. Journal of Geophysical Research: Oceans, 101(C6): 13975–13991, doi: 10.1029/96JC00559

Sharma R, Agarwal N, Momin I M, et al. 2010. Simulated sea surface salinity variability in the tropical Indian Ocean. Journal of Climate, 23(24): 6542–6554, doi: 10.1175/2010JCLI3721.1

Shchepetkin A F, McWilliams J C. 2003. A method for computing horizontal pressure-gradient force in an oceanic model with a nonaligned vertical coordinate. Journal of Geophysical Research: Oceans, 108(C3): 3090, doi: 10.1029/2001JC001047

Shee A, Sil S, Gangopadhyay A, et al. 2019. Seasonal evolution of oceanic upper layer processes in the northern Bay of Bengal following a single Argo float. Geophysical Research Letters, 46(10): 5369–5377, doi: 10.1029/2019GL082078

Shenoi S S C, Shankar D, Shetye S R. 2002. Differences in heat budgets of the near-surface Arabian Sea and Bay of Bengal: implications for the summer monsoon. Journal of Geophysical Research: Oceans, 107(C6): 3052, doi: 10.1029/2000JC000679

Shetye S R, Gouveia A D, Shankar D, et al. 1996. Hydrography and circulation in the western Bay of Bengal during the northeast monsoon. Journal of Geophysical Research: Ocean, 101(C6): 14011–14025, doi: 10.1029/95JC03307

Song Yuhe, Haidvogel D. 1994. A semi-implicit ocean circulation model using a generalized topography-following coordinate system. Journal of Computational Physics, 115(1): 228–244, doi: 10.1006/jcph.1994.1189

Suryanarayana A, Murty V S N, Rao D P. 1993. Hydrography and circulation of the Bay of Bengal during early winter, 1983. Deep-Sea Research Part I: Oceanographic Research Papers, 40(1): 205–217, doi: 10.1016/0967-0637(93)90061-7

Sweeney C, Gnanadesikan A, Griffies S M, et al. 2005. Impacts of shortwave penetration depth on large-scale ocean circulation and heat transport. Journal of Physical Oceanography, 35(6): 1103–1119, doi: 10.1175/JPO2740.1

Thadathil P, Gopalakrishna V V, Muraleedharan P M, et al. 2002. Surface layer temperature inversion in the Bay of Bengal. Deep-Sea Research Part I: Oceanographic Research Paper, 49(10): 1801–1818, doi: 10.1016/S0967-0637(02)00044-4

Thadathil P, Muraleedharan P M, Rao R R, et al. 2007. Observed seasonal variability of barrier layer in the Bay of Bengal. Journal of Geophysical Research: Oceans, 112(C2): C02009, doi: 10.1029/2006JC003651

Thadathil P, Suresh I, Gautham S, et al. 2016. Surface layer temperature inversion in the Bay of Bengal: main characteristics and related mechanisms. Journal of Geophysical Research: Oceans, 121(8): 5682–5696, doi: 10.1002/2016JC011674

Thandlam V, Rahaman H. 2019. Evaluation of surface shortwave and longwave downwelling radiations over the global tropical oceans. SN Applied Sciences, 1(10): 1171, doi: 10.1007/s42452-019-1172-2

Thangaprakash V P, Girishkumar M S, Suprit K, et al. 2016. What controls seasonal evolution of sea surface temperature in the Bay of Bengal? Mixed layer heat budget analysis using moored buoy observations along 90°E. Oceanography, 29(2): 202–213, doi: 10.5670/oceanog.2016.52

Thompson B, Gnanaseelan C, Salvekar P S. 2006. Seasonal evolution of temperature inversions in the north Indian Ocean. Current Science, 90(5): 697–704

Vialard J, Delecluse P. 1998. An OGCM study for the TOGA decade. Part II: barrier-layer formation and variability. Journal of Physical Oceanography, 28(6): 1089–1106, doi: 10.1175/1520-0485(1998)028<1089:AOSFTT>2.0.CO;2

Vialard J, Foltz G R, McPhaden M J, et al. 2008. Strong Indian Ocean sea surface temperature signals associated with the Madden-Julian oscillation in late 2007 and early 2008. Geophysical Research Letters, 35(19): L19608, doi: 10.1029/2008GL035238

Vinayachandran P N. 2005. Bifurcation of the east India coastal current east of Sri Lanka. Geophysical Research Letters, 32(15): L15606, doi: 10.1029/2005GL022864

Vinayachandran P N, Murty V S N, Babu V R. 2002. Observations of barrier layer formation in the Bay of Bengal during summer monsoon. Journal of Geophysical Research: Oceans, 107(C12): 8018, doi: 10.1029/2001JC000831

Vinayachandran P N, Shankar D, Vernekar S, et al. 2013. A summer monsoon pump to keep the Bay of Bengal salty. Geophysical Research Letters, 40(9): 1777–1782, doi: 10.1002/grl.50274

Vinayachandran P N, Yamagata T. 1998. Monsoon response of the sea around Sri Lanka: generation of thermal domes and anticyclonic vortices. Journal of Physical Oceanography, 28(10): 1946–1960, doi: 10.1175/1520-0485(1998)028<1946:MROTSA>2.0.CO;2

Vorosmarty C J, Fekete B M, Tucker B A. 1998. Global river discharge, 1807–1991, V. 1.1 (RivDIS). Oak Ridge: ORNL DAAC, doi:

10.3334/ORNLDAAC/199

Weller R, Farrar J T, Buckley J, et al. 2016. Air-sea interaction in the Bay of Bengal. Oceanography, 29(2): 28–37, doi: 10.5670/oceanog.2016.36

Wyrtki K, Bennett E B, Rochford D J, et al. 1971. Oceanographic Atlas of the International Indian Ocean Expedition. Washington: National Science Foundation

Yu Lisan. 2003. Variability of the depth of the 20°C isotherm along 6°N in the Bay of Bengal: its response to remote and local forcing and its relation to satellite SSH variability. Deep-Sea Research Part II: Topical Studies in Oceanography, 50(12–13): 2285–2304, doi: 10.1016/S0967-0645(03)00057-2

Yu H, Kaufman Y J, Chin M, et al. 2006. A review of measurement-based assessments of the aerosol direct radiative effect and forcing. Atmospheric Chemistry and Physics, 6(3): 613–666, doi: 10.5194/acp-6-613-2006